Telmisartan Reverses Hepatic Steatosis via PCK1 Upregulation: A Novel PPAR-independent Mechanism in Experimental Models of MASLD

Roger Bentanachs[1,3], Patricia Ramírez-Carrasco[1,3], Bianca Braster[4,5], Anastasia Emmanouilidou[4,5], Endrina Mujica[4,5], Maite Rodrigo-Calvo[6], Cristina Rodríguez[7,8], Núria Roglans[1,2,3], Marcel den Hoed[4,5], Juan C. Laguna[1,2,3], Marta Alegret[1,2,3]

[1]Department of Pharmacology, Toxicology and Therapeutic Chemistry, School of Pharmacy and Food Science, University of Barcelona, 08028 Barcelona, Spain.

[2]Spanish Biomedical Research Centre in Physiopathology of Obesity and Nutrition (CIBEROBN), Instituto de Salud Carlos III, 28029 Madrid, Spain.

[3]Institute of Biomedicine IBUB, University of Barcelona, 08028 Barcelona, Spain.

[4]Department of Immunology, Genetics and Pathology, Uppsala University, 75105 Uppsala, Sweden.

[5]SciLifeLab, 752 37 Uppsala, Sweden.

[6]Pathology Department, Center of Biomedical Diagnosis (CDB), Hospital Clinic, 08036 Barcelona, Spain.

[7]Institut de Recerca Sant Pau (IR SANT PAU), 08041Barcelona, Spain.

[8]Spanish Biomedical Research Centre in Cardiovascular diseases (CIBERCV), Instituto de Salud Carlos III, 28029 Madrid, Spain.

Corresponding author: Marta Alegret; alegret@ub.edu. Department of Pharmacology, Toxicology and Therapeutic Chemistry, School of Pharmacy and Food Science, University of Barcelona, Av. Joan XXIII 27–31, 08028 Barcelona, Spain

Abstract

Drug combination and repurposing are potential therapeutic strategies for the treatment of metabolic dysfunction-associated steatotic liver disease (MASLD). Here, we have demonstrated that, in rats, both pemafibrate and telmisartan reverse hepatic steatosis induced by a high-fat, high-fructose diet. Pemafibrate attenuated liver steatosis via a PPARα-mediated increase in fatty acid catabolism, while the antisteatotic response to telmisartan did not rely on PPAR modulation. Our results in rats and in a zebrafish larva model of liver lipid accumulation suggest that part of telmisartan's antisteatotic effects are driven through the blockade of the angiotensin II type 1 receptor, along with a reduction in the expression of several lipogenic genes, which also contributes to some extent. Telmisartan's response is mediated by the upregulation of hepatic phosphoenolpyruvate carboxykinase 1 (PCK1) expression. Liver metabolomic analysis revealed that by increasing PCK1, telmisartan diverted the metabolic flux of fructose from lipid towards glucose synthesis, which was subsequently fueled to the polyol pathway, thereby preserving glucose homeostasis. Moreover, telmisartan increased the hepatic levels of spermine and spermidine, which may counteract the putative detrimental effects caused by the accumulation of metabolites of the polyol route. Targeting different intrahepatic pathways, both PPAR-dependent and independent, the combination of pemafibrate and telmisartan, each at half the individual dose, was equally effective as the full dose of either drug alone to reduce liver lipid accumulation in the rat model. Our findings support the repurposing potential of these drugs, with the additional advantage of addressing both hepatic and cardiometabolic MASLD-associated complications.

Keywords: Liver Steatosis; PPAR; Angiotensin Receptor Blockers; Metabolomics; Phosphoenolpyruvate carboxykinase 1; Gluconeogenesis

Highlights

- Telmisartan reverses hepatic steatosis via PCK1 upregulation, independently of PPARα/Y
- Telmisartan diverts fructose metabolism from lipid synthesis towards gluconeogenesis and polyol pathways
- Pemafibrate effectively reduces liver steatosis through PPARα-mediated mechanisms
- The results support the repurposing of telmisartan and pemafibrate for MASLD management

1. Introduction

Metabolic dysfunction-associated steatotic liver disease (MASLD) is the most prevalent liver disease globally. Recent estimates suggest it affects approximately 38% of adults, and its prevalence is anticipated to continue rising in the coming years [1]. MASLD includes a range of disease states, from the asymptomatic accumulation of triglycerides in the liver without inflammation or hepatocyte enlargement [2](metabolic dysfunction-associated steatotic liver, MASL), to metabolic dysfunction-associated steatohepatitis (MASH), characterized by inflammation, hepatocyte ballooning and a high risk to progress to hepatic fibrosis [3]. Intrahepatic lipid accumulation is the hallmark of the MASLD spectrum and plays a causative role in disease progression [2]. Despite persistence of MASH and advanced fibrosis leading to cirrhosis and hepatocellular carcinoma, the overall risk of mortality already increases from the early stages of MASLD, with cardiovascular disease (CVD) being the leading cause of death [4,5]. Thus, the presence of MASLD has been associated with a high risk of both fatal and non-fatal CVD events [6]. Current pharmacotherapy is limited and given the high prevalence but low liver-related mortality, MASLD treatment must prioritize safety, making drug repurposing an ideal therapeutic strategy.

Hypertension is one of the risk factors that have been related to the pathogenesis of both MASLD and atherosclerotic CVD [7]. Around 50% of patients with hypertension also have MASLD, and increased activity of the renin-angiotensin-aldosterone system (RAS) may be a pathogenic mechanism connecting both diseases [8]. In line with this, a common gain-of-function variant in the gene encoding angiotensin II type 1 receptor (*AGTR1*), AA1166C, has been associated with increased risk of MASLD and fibrosis [9]. The liver expresses all the components of the system, and activation of hepatic RAS results in steatosis, insulin resistance, inflammation and necrosis [10]. Therefore, RAS inhibition with an angiotensin II receptor blocker (ARB) like telmisartan (Tel), an effective anti-hypertensive agent, emerges as a promising therapeutic approach. Small clinical trials have reported improvements in MASLD markers with Tel treatment [11,12]. Unlike other ARBs, Tel has may provide an additional protection against MASLD, thanks to its putative peroxisome proliferator-activated receptor Y (PPARY) agonistic properties [13]. Although ARBs reduce insulin resistance and hepatic fibrosis in animal models of MASLD [14], their potential benefit against hepatic steatosis and the mechanism of action are not fully understood.

Since MASLD is a complex disease with relevant extra-hepatic comorbidities, a multidisciplinary treatment approach is recommended to reduce both hepatic and cardiometabolic complications. Combination therapy with drugs targeting different pathogenic pathways may be a better strategy than monotherapy, due to potential synergistic effects and to reduced toxicity related to the use of lower doses of individual drugs. Specifically, the combination of drugs that simultaneously activate several PPAR isotypes may be more beneficial than targeting only a single isotype [15]. Recently, we implemented a MASL model by feeding female Sprague-Dawley rats with a high-fat diet supplemented with liquid fructose (HFHFr) [16]. In this model, we examined the liver-targeted effects of pemafibrate (PemA), a selective PPARα modulator approved for the management of hypertriglyceridemia, a common comorbidity in MASLD patients [17]. PemA is currently being evaluated in a clinical trial for MASLD and hypertriglyceridemia [18].

Here, we assessed the antisteatotic effects of Tel, alone and in combination with PemA, to evaluate the repurposing potential for MASLD of these two drugs, which present an adequate safety profile in humans. Our findings in the HFHFr rat model confirm and extend our previous results with PemA, showing its efficacy in reversing liver steatosis by a PPARα-mediated increase in fatty acid catabolism, even at lower doses than those reported for its clinical use. We also show the ability of Tel alone to ameliorate hepatic steatosis in two experimental

MASLD models. The antisteatotic effect of Tel was PPAR-independent and was related to the upregulation of liver phosphoenolpyruvate carboxykinase 1 (PCK1) expression, leading to a diversion of the hepatic flux of metabolites from lipid synthesis towards gluconeogenesis and polyol pathways.

2. Materials and methods

2.1. Rat MASL model and experimental design

Two-month-old female Sprague-Dawley rats weighting 149 ± 4 g (Envigo, Barcelona, Spain) were housed two per cage under conditions of constant humidity (40–60 %) and temperature (20–24 ºC), with a light/dark cycle of 12 h. Rats were randomly divided into five groups (n = 8 each): (i) control (CT), fed a regular chow diet (2018 Teklad Global rodent diet, Envigo, Madison, USA) with free access to water; (ii) HFHFr, fed a high-fat diet (Teklad Custom Diet 180456, Envigo, Madison, USA) [16], with free access to a 10% w/v fructose solution; (iii) PemA, fed the HFHFr diet plus PemA at a dose of 0.5 mg/kg/day, (iv) Tel, fed the HFHFr diet plus Tel at a dose of 10 mg/kg/day, and (v) combination of PemA and Tel (P+T, at a dose of 0.25 and 5 mg/kg/day, respectively). CT and HFHFr groups were fed on the respective diets for three months. The PemA, Tel and P+T groups received the HFHFr diet for two months, followed by an additional month in which rats received the indicated drugs incorporated into the diet at a concentration providing the daily doses. Doses, route, and length of drug administration were chosen based on previous studies by our group and others. Solid food and liquid consumption were controlled three times a week, and body mass was recorded once a week. 3 animals were excluded from the study due to signs of distress, in accordance with humane endpoints and ethical guidelines.

At the end of the treatment, rats were fasted for 2 h, and tail vein blood samples were obtained to measure triglyceride and cholesterol levels using an Accutrend Plus system meter (Cobas, Roche Farma, Barcelona, Spain), while glucose levels were determined using a Nesira glucometer (Acofarma, Barcelona, Spain). The rats were then immediately anesthetized as described [16] and blood was collected into micro-tubes (Sarstedt AG & Co., Nümbrecht, Germany) through cardiac puncture. Serum was obtained by centrifugation at 10,000x g for 5 min at room temperature. Samples of liver, brown adipose tissue, subcutaneous and perigonadal white adipose tissue (WAT) were collected, immediately frozen in liquid nitrogen, and stored at -80 ºC.

2.2. Serum analytes.

Serum insulin, leptin, and fibroblast growth factor 21 (FGF21) concentrations were determined using specific ELISA kits from Millipore (Insulin: EZRMI-13K, Leptin: EZRL-83K, FGF21: EZRMFGF21-26K; Billerica, MA, USA). Adiponectin levels were detected by an ELISA kit from Proteintech (KE20016; Rosemont, IL, USA). Serum non-esterified free fatty acids (NEFA) were determined by a colorimetric kit from Biooscientific (5620-01; Austin, TX, USA). The kits to assess alanine (ALT) and aspartate aminotransferase (AST) kinetics were acquired from Spinreact (41270 and MI41264 respectively, Girona, Spain). Serum angiotensin 1-7 (ang (1-7)) levels were assessed using an ELISA kit from Universal Biologicals (RD-Ang1-7-Ra, Cambridge, UK). The insulin sensitivity index (ISI) was calculated as described previously [19].

2.3. Fatty acid β-oxidation activity

Total fatty acid β-oxidation was determined as described by Lazarow [20], using 30 µg of post-nuclear supernatant from the liver samples.

2.4. Liver Lipid Content

Hepatic triglyceride (TG) and cholesterol were extracted as described by Qu et al. [21] and

determined using colorimetric assay kits from Spinreact (1001311 and MD41021, respectively, Girona, Spain).

2.5. Hepatic glycogen contents

The hepatic concentration of glycogen was determined using the colorimetric Glycogen Assay Kit MAK016 (Sigma-Aldrich, St. Louis, MO, USA), following the manufacturer's instructions.

2.6. Histological studies and pathology assessment

Paraffin-embedded livers were cut into 5 µm sections and stained with hematoxylin and eosin (H&E) or Sirius Red, and OCT-embedded liver sections stained with Oil-Red O (ORO). Images were acquired with a Leica DMSL microscope equipped with a DP72 camera (Leica Microsistemas, Barcelona, Spain) and analyzed using Image J 1.49 software (National Institutes of Health, Bethesda, MD, USA). The area positive for ORO staining was normalized to the total area. All procedures were carried out in the Animal Histopathology Laboratory at the University of Barcelona. Disease stage was evaluated based on the Nonalcoholic Fatty Liver Disease (NAFLD) activity score (NAS) system [22].

2.7 Measurement of fatty acid methyl esters in liver TGs.

Fatty acid methyl esters (FAMEs) from liver TGs were determined by Gas Chromatography-Mass Spectrometry (GC/MS-EI) as described in detail elsewhere [17].

2.8. Fecal bile acids analysis

The concentrations of 10 bile acids (BA) (cholic acid, chenodeoxycholic acid, deoxycholic acid, lithocholic acid, ursodeoxycholic acid, α-muricholic acid, β-muricholic acid, hyocholic acid, hyodeoxycholic acid, and murideoxycholic acid) in rat feces were determined by ultra-high-performance liquid chromatography coupled to tandem mass spectrometry (UHPLC-MS/MS) as described previously [17].

2.9. Western blot analysis

Tissue samples for western blot analysis were homogenized with a Polytron PT 1200E homogenizer in lysis buffer containing proteases, phosphatases, and deacetylase inhibitors, and incubated for 1.5 h at 4°. Samples were then centrifuged at 15,000 x g for 15 min at 4 ºC, and supernatants were collected. Protein concentrations were determined by the Bradford method [23]. Western blots were carried out using 10-30 µg of total protein. After SDS-polyacrylamide gel electrophoresis, proteins were transferred onto Immobilon polyvinylidene difluoride transfer membranes (Millipore, Billerica, MA, USA), and blocked for 1 h at room temperature with blocking solution (SP 7000; WestVision™, Newark, CA, USA). Membranes were then incubated with specific primary antibodies (Table S1). Detection was performed using the Immobilion Western HRP substrate Peroxide Solution® (Millipore, Billerica, MA, USA). To confirm the uniformity of protein loading, blots were incubated with anti-vinculin (Santa Cruz Biotech, Dallas, TX, USA) antibody as a control for total protein extracts.

2.10. Mas receptor liver protein levels.

Liver Mas receptor (MasR) protein levels were detected using a specific ELISA kit from LSbio (LS-F66779, Newark, CA, USA) following the manufacturer's protocol.

2.11. Ubiquitinated PCK1

Ubiquitinated PCK1 relative protein levels were detected using the Signal-Seeker™ Ubiquitination kit (BK161-S, Cytoskeleton Inc, Denver, CO, USA), following the manufacturer's protocol for liver tissue. Briefly, a co-immune precipitation was performed from liver tissue

extracts using either control beads or ubiquitination affinity beads. Subsequently, the enriched and whole protein populations were analyzed by western blot using a specific primary antibody against PCK1.

2.12. RT-qPCR analysis

Total RNA was extracted from rat tissues (50-100 mg of each sample) using a phenol-based method according to the manufacturer's instructions (Trisure® reagent, Bioline, Meridian Biosciences, Cincinnati, OH, USA). RNA concentration was assessed using absorbance at 260 nm, while the 260/280 nm absorbance ratio was used to quantify RNA quality. For real-time polymerase chain reaction (RT-qPCR), 1 µg RNA was reverse transcribed into cDNA using the Moloney Murine Leukemia Virus Reverse Transcriptase (MLV-RT; Invitrogen, Carlsbad, CA, USA), random hexamers (Roche, Meylan, France) and dNTP (Sigma-Aldrich, St. Louis, MO, USA). Specific mRNAs were assessed in the StepOnePlus Real-Time PCR System Thermal Cycling Block (Applied Biosystems, Foster City, CA), using 100 µM of each specific primer, 10-100 ng of cDNA, and Maxima SYBR Green qPCR Master with ROX (K0253, ThermoFisher, Waltham, MA, USA). mRNA expression was calculated using the recommended $2^{-\Delta\Delta}$Ct method. β-actin was used as a housekeeping gene to normalize the results for the rat and zebrafish studies. The primer sequences, Genbank TM accession numbers and PCR product lengths are listed in Table S2.

2.13. Untargeted metabolomic analysis

The metabolomic analysis was conducted at oloBion SL, an omics bioscience laboratory (Parc Cientific de Barcelona, Spain). Tissue sample preparation involved homogenization with cold methanol using a grinder, followed by the addition of methyl tert-butyl ether containing an internal standard. The mixture was shaken and subsequently supplemented with 10% methanol. After an additional shaking step, the samples were centrifuged to separate the phases.

For metabolomic profiling, two aliquots of 70 µL of the bottom aqueous phase were collected and processed. The first aliquot was evaporated to dryness and resuspended in acetonitrile/water (containing an internal standard). The solution was shaken, centrifuged, and analyzed using a hydrophilic interaction liquid chromatography. The second aliquot was mixed with isopropanol/acetonitrile (1:1) mixture, shaken, centrifuged and the supernatant was evaporated and resuspended in 5% methanol containing internal standards. After shaking and centrifuging, the sample was analyzed using a reversed-phase liquid chromatography.

Chromatographic separation of polar metabolites was performed on Waters ACQUITY UPLC C18 BEH Amide and ACQUITY UPLC HSS T3 columns, both maintained at 45 °C. The system was coupled to an Agilent 1290 Infinity UHPLC (Agilent Technologies) and a ZenoTOF 7600 system (SCIEX). Sample injection was performed at 4 µL for both electrospray ionization positive and negative modes.

For metabolite identification, the acquired data were processed and analyzed using oloMAP2.0 and the analysis and interpretation was performed with oloMAP Portal 6.1, an advanced data visualization and interpretation platform for omics datasets. The metabolite filters used for chemical and pathway enrichment analysis were $p < 0.05$ and $|\log2\ FC| > 0.5$.

2.14. Zebrafish MASLD model

Adult zebrafish (*Danio rerio*) were housed in systems with recirculating filtered water at 28.5°C (Aquaneering, San Marcos, CA, USA) on a 14/10 h light/dark cycle. We used fish with transgenically expressed, fluorescently labelled hepatocytes (*Tg(-2.8fabp10a:EGFP)*^{as3TG}) (European Zebrafish Resource Center, EZRC [24,25]) in the AB background

(EZRC; http://zfin.org/ZDB-GENO-960809-7). To generate offspring for experiments, fish homozygous for the fluorescently labelled transgene were outcrossed with wild type AB fish. Eggs were allowed to develop in an incubator at 28.5 °C. At 1 day post fertilization (dpf), unfertilized eggs and dead embryos were removed, and remaining embryos were distributed at 60 per Petri dish. At 5 dpf, larvae from the different crosses were proportionally distributed into experimental tanks at a density of 30 larvae per 1 L tank containing 300 mL of water. Tanks were then randomly assigned to experimental conditions, i.e., the standard fed group (SF), fed 5.43 mg dry food twice per day (zebrafeed <100 µm; SPAROS, Portugal); the overfed plus fructose (OF+FR) or overfed plus glucose (OF+GL) groups, fed on 3x more, i.e., 16.3 mg of dry food twice a day that were additionally exposed to 3% fructose or glucose in the water; OF+GL treated with Tel from 8 to 10 dpf at 0.4 (Tel 0.4µM) or 2 (Tel 2µM) µM. Tanks were fed approximately at 9:00 and 15:30 and the different dietary regimens started at 5 dpf in the afternoon and were continued until the afternoon of 7 dpf (in 5 to 8 dpf experiments) or until the afternoon of 9 dpf (in 5 to 10 dpf experiments). Tel was dissolved in DMSO to the desired working concentrations, maintaining a final DMSO concentration of 0.08% in all experimental tanks. The same concentration of DMSO was used, when necessary, in untreated tanks. A full water exchange was performed once a day, and drug or DMSO solutions were renewed daily.

2.15. CRISPR/Cas9-induced mutations and presumed loss-of-function (pLOF) model in zebrafish

Based on European Bioinformatics Institute (EMBL-EBI) and the *Danio rerio* genome version from (www.ensembl.org/index.html) we identified the human orthologs and relevant alternative transcripts for the human *AGTR1* (i.e., *agtr1a* - ENSDARG00000018616 and *agtr1b* - ENSDARG00000045443) and *PCK1* genes (*pck1* - ENSDARG00000013522). CRISPOR (v4.98 and v4.99; http://crispor.tefor.net) online tool [26] was used to identify single guide RNA (sgRNA) in the coding region of these zebrafish genes that meet the following criteria: (1) target early exons (first quarter of the coding regions); (2) are shared across all relevant alternative transcripts; (3) avoid DNA variants included in the reference genome; (4) have a high 'azimuth score'; and (5) have no or few predicted off-target sites with zero to four mismatches (Table S3). Following the same criteria, an identical sgRNA from (ZDB-CRISPR-180314-3; www.zfin.org) to target sparse/Kit receptor tyrosine kinase-a gene, *Kita* (ENSDARG00000043317) was used as a control gene. Specifically, to generate *agtr1a/b* crispants both orthologs, *agtr1a* and *agtr1b* plus *kita*, were targeted simultaneously (Fig. S3). *pck1* crispants were generated by targeting the only protein-coding transcript of the zebrafish ortholog at two sites, along with *kita* (Fig. S3). Finally, controls were only targeted at *kita*. All genes were targeted using the Alt-R CRISPR/Cas9 system (IDT, Belgium) [28]. crRNAs with the selected target sequences and Alt-R CRISPR/Cas9 tracrRNA were resuspended at 100 µmol/L in Duplex Buffer (IDT, Coralville, IA, United States) and stored at –20°C for later use. To prepare 50 µmol/L sgRNA, equal volumes of the 100 µmol/L crRNA and tracrRNA solutions were combined. This mixture was then annealed by heating to 95 °C for 5 min, gradually cooled at a rate of 0.1 °C per sec to 25 °C, held at 25 °C for 5 min, and quickly chilled to 4 °C. The resulting sgRNA solution was stored at –20 °C until needed. On the day of microinjection, injection mixtures were freshly prepared for each genotype: for *agtr1a/b* crispants, 1 µl of *kita* sgRNA, 1 µl of *agtr1a* sgRNA, and 1 µl of *agtr1b* sgRNA were combined; for *pck1* crispants, 1 µl of *kita* sgRNA, 1 µl of *pck1_1* sgRNA, and 1 µl of *pck1_2* sgRNA were used; and for *kita* controls, 3 µl of *kita* sgRNA was added. Each mixture was then combined with 2.4 µl of Alt-R Cas9 (IDT) and 4.6 µl of ultra-pure H2O. Mixes were incubated at 37 °C for 5 min and 1 µl of phenol red (Sigma-Aldrich-Merck, Solna, Sweden) was added as a visual injection aid.

For micro-injections, eggs from all clutches produced in the same round of crossings were pooled and then randomized into two groups to generate *agtr1a/b* or *pck1* crispants and controls. Microinjections into the cell or into the yolk close to the cell were performed at the

single-cell stage using standard micro-injection equipment. Eggs were kept and sorted at 1 dpf as described previously. At 5 dpf, the efficiency of CRISPR/Cas9 gene editing was evaluated by observing pigmentation patterns under a stereo microscope. Since *kita* disruption leads to a reduction or absence of melanocyte presence and migration, larvae showing pigmentation were excluded from further analysis. After that, the survival rate for each genotype was recorded (Fig S3) and the remaining larvae from the different crossing rounds were proportionally distributed to experimental tanks at a 50:50 ratio of crispants and controls, to blind the imaging procedure and to reduce the influence of tank-specific effects. Tanks were randomly assigned to either OF+GL or Tel 2µM conditions as described previously.

For the pLOF model experiments, larvae were categorized by genotype according to fragment length analysis (as described by Varshney et al [29]), using larval DNA. Detailed procedures of DNA obtention, amplification of the sgRNA target region, DNA-analyzer reaction mix, chromatograms and analysis are described in Mazzaferro et al. [30]. An R script generated in-house was used to discriminate between mutated larvae and controls based on the wild-type length, which was defined as the mean of the fragment size in the un-injected siblings ± 0.4 base pairs. Larvae were classified as mutated at *agtr1* if both primer sets (one corresponding to each ortholog) showed a relative wild-type peak area < 0.50. Larvae were considered mutated at *pck1* if at least one primer set met this criterion. Larvae were considered controls when the relative wild-type peak area was > 0.80 at all targeted sites (except *kita*).

2.16. Imaging of zebrafish larvae

On the morning of 8 dpf or 10 dpf, larvae were washed twice with water and incubated for 30 min at 28.5 °C in 12.5 µmol/L monodansylpentane (MDH) (Abcepta, San Diego, CA, USA) in PBS at 0.8 µl/larva to stain neutral lipids. After incubation, larvae were anesthetized by adding tricaine to a final concentration of 230 µmol/L and were placed individually into wells of a 96-well plate. From there, they were automatically aspirated and oriented in a glass capillary using an Autosampler and Vertebrate Automated Screening Technology (VAST) BioImager (Union Biometrica, Aalst, Belgium) built on the stage of a Leica DM6 B fluorescence microscope with a DFC9000 GT sCMOS camera (MicroMedic A/B, Stockholm, Sweden) and its software (Leica Application Suite X V3.7.3.23245). Once larvae were positioned, we first acquired full body images, one every 30° of rotation around the longitudinal axis of the body using the VAST BioImager's bright-field camera. After that, a z-stack of 75 optical sections of the liver was acquired using a 10X objective (HCX APO L NA 0.30 U-V-I) and a GFP filter for the hepatocytes, and a 405 filter for the MDH-stained lipids. After imaging, larvae were dispensed into a 96-well PCR plate and euthanized by prolonged exposure to tricaine and ice. Water was removed and samples were stored at –20°C until further analysis if necessary. Using the imaging data, body size traits (whole-body length, dorsal area, lateral area) and hepatic traits (liver size, number and area of lipid objects) were quantified by custom-written deep learning algorithms [27].

2.17. Statistical analysis

Results obtained in the rat HFHFr model are expressed as mean ± standard deviation (SD). Significance was established by t-test or one-way ANOVA multiple comparisons test and a Šidák's post-hoc test for selected comparisons (GraphPad Software version 10, San Diego, CA, USA). When the SD of the groups was different according to the Brown–Forsythe test, the data were log-transformed and the parametric test was rerun, or the corresponding non-parametric test was applied. Zebrafish data management was performed with STATA (v18; StataCorp, USA) except for the fragment length analysis, which was performed with R (v 4.3.3). For zebrafish studies, deep-learning image-analysis results (outcomes) were inverse normally transformed to a mean of 0 and SD of 1 before the analysis. Linear regression analysis was

performed to examine the effect of gene and/or treatment effects on traits of interests, adjusting the results for the time of the day at which larvae were imaged and for batch (experimental round). Effects on dorsal and lateral area were additionally adjusted for body length as a covariable. T-tests were used to compare the mortality from day 1 to 5 between *agtr1a/b* or *pck1* crispants and controls, or between treated and untreated tanks in pLOF experiments from 8 to 10 dpf. For the metabolomics study, the statistical analysis was performed using oloMAP 2.0. In all cases, statistical significance was defined at $P < 0.05$.

3. Results

3.1. Pemafibrate and telmisartan both reduce hepatic triglyceride content and steatosis

As we previously described [16], rats that received a HFHFr diet consumed fewer calories from solid food than control rats. Treatment with PemA (0.5 mg/kg/day), Tel (10 mg/kg/day), or their combination at half the individual dose of each drug, did not alter energy intake from solid or liquid sources compared with untreated rats (Fig. 1A). At the end of treatment, body weight was similar between groups (Fig. 1B). While circulating cholesterol levels were similar, blood TG levels were increased by the HFHFr diet (x1.4) and unaffected by drug treatment (Fig. 1C, D). Blood glucose levels and serum insulin concentrations were similar across groups, but the insulin sensitivity index (ISI) was lower in HFHFr than CT fed rats (Fig. 1E-G). PemA, alone or combined with Tel, marginally increased the ISI value ($p=0.08$).

ORO staining of liver samples showed that treatment with PemA or Tel completely abolished HFHFr diet-induced hepatic steatosis. Combined treatment with both drugs induced a similar reduction (Fig 2A). Moreover, these treatments significantly reduced all fatty acid species analyzed, except arachidonic acid (Fig. S1). H&E staining of liver samples showed that these treatments abolished early signs of damage caused by the HFHFr (Fig. 2B). Sirius Red stains of liver sections from all experimental groups revealed no evidence of fibrosis (Fig 2C). The NAS score and all subcomponent scores (steatosis, inflammation and ballooning) were reduced by drug treatment (Fig. 2D-E). In line with similar circulating AST and ALT levels in HFHFr and CT, none of the oxidative stress or inflammation/fibrotic markers were upregulated, precluding the classification of this model as MASH (Fig. 2F-H). However, absolute and liver to body weight ratio were higher in HFHFr than CT fed rats (x 1.2), and in PemA or P+T *vs.* HFHFr (x 1.4 and 1.3, respectively). Tel alone did not alter these parameters (Fig. 2I-J). Our results also showed that liver cholesterol levels were similar among the five groups, while hepatic TG levels were increased by the HFHFr diet (x 3.9-fold) and similarly reduced by all therapeutic interventions (Fig 2 K, L).

3.2. Pemafibrate reduces liver triglycerides by increasing fatty acid catabolism

We have previously described that PemA, at a dose of 1 mg/kg/day, abrogated liver lipid accumulation in HFHFr-fed rats by a PPARα-dependent increase in fatty acid catabolism [17]. As described above, at 0.5 mg/kg/day PemA also exhibited a strong antisteatotic effect. Hence, we investigated if PemA, Tel, and P+T, shared the same mode of action. Our results confirmed that, in HFHFr-fed animals, PemA alone or combined with Tel, significantly increased hepatic β-oxidation activity to a similar degree (Fig 3A). Accordingly, hepatic expression of genes coding for rate limiting enzymes of mitochondrial (liver-carnitine palmitoyl transferase I, l-*Cpt1*), and peroxisomal (acyl-CoA oxidase, *Aco*) β-oxidation, as well as pyruvate dehydrogenase kinase 4 (*Pdk4*), a sensitive marker of fatty acid oxidation, were all increased by PemA (Fig 3B). In addition, the mRNA levels of adipose triglyceride lipase (*Atgl*), the rate limiting enzyme of triglyceride hydrolysis that is positively associated with hepatic β-oxidation, were increased by PemA (Fig 3B). In turn, only PemA increased serum levels of FGF21 (Fig 3C), a well-known

PPARα target, and decreased hepatic protein levels of ketohexokinase (KHK), an essential enzyme for fructose metabolism whose expression is downregulated by PPARα activation (Fig 3D). Unlike PemA [17], Tel did not affect the concentration of fecal BA compared to rats fed on HFHFr (Fig. S2), suggesting this mechanism does not mediate its effect on liver metabolism.

We also examined the effects of PemA, Tel and P+T on two proteins that regulate plasma TG levels, angiopoietin-like protein 3 (ANGPTL3) and patatin-like phospholipase domain-containing protein 3 (PNPLA3). As shown in Fig 3B, no treatment influenced *Pnpla3* expression, although PemA and P+T tended to increase ANGPTL3 serum levels (Fig 3E).

3.3. Telmisartan does not activate PPARY or induce adipose tissue browning in HFHFr fed rats

After having confirmed that PemA reduced liver TG accumulation by enhancing fatty acid catabolism and that Tel did not share this mode of action, we focused on Tel's effects on other metabolic pathways. Tel has been shown to activate PPARY [13] and induce adipose tissue browning in HFD-fed mice [28]. However, Tel administration to HFHFr rats did not alter the mRNA levels of *Ppary2* or its target gene *Cd36* either in liver or perigonadal WAT (pWAT, Fig. 4A). Moreover, pWAT expression of the gene encoding adiponectin (*AdipoQ,* Fig. 4B) as well as its serum levels (Fig. 4C) remained unaltered. Interestingly, pWAT relative weight was increased by the HFHFr diet, and treatment with Tel totally prevented this increase. Conversely, the higher relative weight of subcutaneous WAT (sWAT) induced by the diet was not altered by Tel, and brown adipose tissue (BAT) relative weight was similar in the three groups of treatment (Fig. 4D). In agreement with reduced adiposity, the NEFA serum levels were also significantly reduced in Tel treated rats (Fig. 4E). The efficacy of Tel in reducing pWAT weight prompted us to study thermogenic gene expression in this specific depot. The results showed that only the mRNA levels of uncoupling protein 1 (*Ucp1*) were significantly upregulated by Tel treatment, but results were not confirmed at the protein level (Fig. 4F).

3.4. Telmisartan reverses HFHFr diet-induced ACE2 downregulation without altering Ang (1-7) serum levels

As Tel is an antagonist of AGTR1, we examined the expression of local components of the classical and alternative RAS in the liver. The mRNA levels of *Agtr1* were reduced by the HFHFr diet, and this response was reversed by Tel treatment (Fig. 5A), without altering protein levels (Fig. 5B-C). Next, we focused on the alternative RAS pathway. Despite *Ace2* expression being similar (Fig. 5A), its protein levels were downregulated by the HFHFr diet (Fig. 5B) and increased after Tel treatment (Fig. 5C). However, serum levels of ang (1-7) were not modified by the diet or the drug treatment (Fig. 5D), and liver levels of MasR protein also remained unaltered in the three conditions (Fig. 5E). Moreover, the ACE2/Ang (1-7)/MasR axis activates Akt and 5' AMP-activated protein kinase (AMPK) signaling [29], but our results did not show evidence of changes in the phosphorylation of these proteins (Fig. 5C).

3.5. Telmisartan does not affect hepatic expression of key lipogenic transcription factors.

As shown in Fig. 6A, the liver mRNA levels of several enzymes involved in *de novo* lipogenesis (DNL) tended to decrease with Tel treatment (Fig 6A), with a significant effect observed only in ATP citrate lyase (ACLY) and FAS protein levels (Fig 6B). However, the expression of the lipogenic transcription factor carbohydrate response element binding protein β (*Chrebpβ*) and its target gene liver-pyruvate kinase (*l-Pk*), were not significantly modified (Fig 6A). Similarly, protein levels of the mature form of sterol response element binding protein 1c (SREBP-1C) remained unaltered (Fig. 6B).

3.6. Untargeted metabolomic: telmisartan causes a shift toward hepatic gluconeogenesis

To gain insight into the mechanisms by which Tel reduces hepatic lipid accumulation, we

performed untargeted metabolomics in hepatic samples from control, HFHFr and Tel-treated rats. A principal component analysis (PCA) plot (Fig. 7A) showed that quality control (QC) samples were highly clustered, indicating test stability and data reliability. We also observed some clustering by exposure, with maximal separation when data were analyzed by unsupervised partial least squares discriminant analysis (PLS-DA), as shown in Fig. 7B. The results showed proper discrimination of the CT group, while HFHFr and Tel partially overlapped, suggesting that diet is the main factor altering the rat liver metabolite profile.

A total of 348 metabolites were identified, and those with $|Log_2 FC| > 0.5$ and P value<0.05 are shown in the Volcano plots (Fig. 7C-D). 74 differential metabolites were detected between HFHFr *vs.* CT, of which 59 were downregulated and five upregulated. When comparing Tel *vs.* HFHFr, four metabolites were downregulated and 20 upregulated. Pathway analysis was performed by over-representation analysis (ORA), and the average log_2 FC of each pathway was calculated using the metabolite InChIKeys and the ChEBI and Reactome databases. In HFHFr *vs.* CT comparison (Fig 7E), most of the metabolites pertaining to gluconeogenesis/glycolysis, pyruvate metabolism and citric acid cycle pathways were downregulated. Importantly, the Tel *vs.* HFHFr comparison showed the opposite enrichment pattern (Fig. 7F), with Tel mostly restoring the metabolomic profile to resemble that of CT animals.

Accordingly, Fig. 8 shows the metabolites most affected by Tel. As expected, Tel was the most upregulated compound, indicating that the drug has been absorbed and is present in the liver of treated animals. In addition, metabolites pertaining to the above cited pathways, like 2/3 phosphoglyceric acid, phosphoenolpyruvic acid, malic acid, fumaric acid and maleic acid, were significantly downregulated by HFHFr and upregulated by Tel. Moreover, the increased levels of fructose, sorbitol and N-acetylgalactosaminitol in the liver of Tel-treated rats suggest an activation of the polyol pathway, while levels of oxidated (GSSG) or reduced (GSH) glutathione were not altered by HFHFr or Tel. Metabolites involved in the pentose phosphate pathway (PPP) and purine/pyrimidine metabolism, such as nicotinamide, xanthine, uridine, uracil ribose-1-phosphate and AMP, were increased by Tel, along with the polyamines spermine and spermidine.

3.7. Telmisartan increases hepatic PCK1 protein levels without modifying its expression

Results from the metabolomic analysis prompted us to examine the effects of Tel on the first rate-limiting enzyme for gluconeogenesis, PCK1. We found a significant reduction of *Pck1* mRNA levels in liver samples of HFHFr (Fig. 9A), in line with our previous results showing that this diet decreases hepatic PCK1 protein levels [16]. In contrast, we found a significant increase in PCK1 protein levels after Tel treatment (Fig. 9B), while no such effect was observed in PemA or P+T. Notably, the protein level changes in Tel occurred without alterations in *Pck1* mRNA expression. Thus, we explored if Tel affects mechanisms involved in PCK1 protein stability.

We observed no changes expression of the E3 ligase UBR5, which enhances PCK1 degradation by ubiquitination [30] (Fig. 9A). GSK3β phosphorylation may lead to PCK1 ubiquitination and degradation, whereas SIRT1 deacetylates PCK1 and enhances its gluconeogenic activity [31]. Neither GSK3β phosphorylation at Ser9 nor SIRT1 protein levels were modified in Tel *vs.* HFHFr (Fig. 9C). Moreover, when hepatic polyubiquitinated proteins from the two groups were purified using specific affinity beads, western blot analysis revealed a parallel increase in the levels of both polyubiquitinated and total PCK1 in samples from Tel-treated rats (Fig. 9D).

Increased liver PCK1 protein levels suggest enhanced gluconeogenesis after Tel treatment. However, since Tel did not influence blood glucose or serum insulin levels (Fig 1), we next examined hepatic glycogen content. As shown in Fig. 9E, glycogen concentration in liver samples from the three groups did not differ significantly.

3.8. Telmisartan has ATR1 and PCK1 dependent antisteatotic effects in zebrafish larvae

To explore which proteins mediate the antisteatotic effect of Tel in a more time-efficient manner, we turned to a zebrafish MASLD model. To establish the optimal MASLD model, we first compared image-based liver fat content in three groups: one group of standard-fed larvae (SF), and two overfed (OF) groups, that received three times the standard diet from day 5 to 10, with water supplemented with either 3% w/v glucose (OF+GL) or 3% w/v fructose (OF+FR). Using image-based quantification of liver fat content and whole-body size in live 10-day-old larvae (Fig. S4), we showed that both dietary-challenged groups has significantly more liver fat than the SF group. The steatotic effect was most pronounced in OF+GL, which were additionally longer, larger, and had a larger liver than SF (Fig. S4 A, D). Hence, we selected the OF+GL model to test the antisteatotic effects of Tel in zebrafish larvae.

Since a significant increase in steatosis is already evident by 8 dpf (Fig. S4B) and to align with a treatment approach similar to the rat model, we treated OF+GL fed larvae with 0.4 or 2 µM Tel from 8 to 10 dpf (Fig. 10A). Compared with untreated OF+GL controls, 2 µM Tel significantly decreased liver fat content and marginally reduced hepatomegaly, without causing significant effects on mortality (Fig. 10B). Tel treatment also resulted in a small but significantly reduced body length and restored the increase in dorsal and lateral area caused by OF+GL (Fig. 10C). Although the liver results presented are not adjusted for length to avoid potential bias, Tel effects persisted after adjusting for body length (data not shown).

Having confirmed the antisteatotic effect of Tel in zebrafish larvae, we aimed to gain insights into the underlying mechanism by testing the consequences of disrupting *atgr1*, the pharmacological target of Tel, and *pck1*, which emerged as one of the most relevant molecular nodes in the rat study on the effect of Tel treatment. One human gene at a time, we used CRISPR/Cas9 to target all relevant transcripts of zebrafish orthologs (Fig. S3). In targeted larvae as well as sibling controls, the control gene *kita* – which affects pigment – was also disrupted, to ensure both groups experienced micro-injections at the single cell stage, DNA editing and DNA repair. The absolute amount of micro-injected Cas9 and gRNA was the same in targeted larvae and controls. Survival from 1 to 5 dpf was the same in *agtr1a/b* or *pck1* targeted larvae and *kita* controls. On day 5, targeted larvae and controls were randomly distributed 50/50% in 1L tanks, at 30 larvae per tank. All larvae were fed OF+GL up to 10 dpf. Half the tanks were treated with 2 µM Tel from 8 to 10 dpf (Fig. 11A). CRISPR/Cas9-induced *agtr1a/b* mutants displayed reductions in liver fat, liver area, and both dorsal and lateral body area whereas *pck1* mutation did not produce any effect (Fig. 11B-D). Tel's effect on liver lipid content was similar in *kita* controls as compared with OF+GL larvae that had not undergone DNA editing (Fig. 11B,C). However, when the *agtr1a/b* mutants were treated with 2µM of Tel, its antisteatotic effect was attenuated, showing non-significant modifications on liver fat (−0.273 ± 0.227) and liver area (-0.392 ± 0.279) (Fig. 11B) compared to *agtr1a/b* mutants alone. Similarly, *pck1* mutation led to the abolishment of Tel liver lipid lowering effect showed on control larvae (−0.260 ± 0.455 *vs. pck1* mutants alone) (Fig. 11C). These results, together with data obtained in rat liver, point to a role of PCK1 in the regulation of hepatic lipid contents.

4. Discussion

MASLD, formerly known as NAFLD, is the most common chronic liver pathology, with a global prevalence projected to rise to 55.4% by 2040 [1]. The rising trend in MASLD prevalence emphasizes the need for early diagnosis and drug screening. In this context the recent FDA approval of resmetirom is an important step forward [32]. Still, concerns remain about its high cost and limited efficacy, with nearly 70% of patients being non-responders [33]. Moreover, resmetirom has been approved for patients with hepatic fibrosis grade 2/3, while drugs targeting earlier stages of the disease could be a more effective approach to prevent MASLD

progression. Therefore, more drugs are needed, to be used either alone or in combination treatments. To date, most new compounds studied for MASLD treatment failed in clinical trials for several reasons, including safety issues [34]. Thus, repurposing of drugs with a well-known and acceptable side-effect profile in humans may be a good, safe and economic option.

In the present study, we examined the repurposing potential of the single or combined administration of a lipid-lowering and an antihypertensive drug (PemA and Tel) for the treatment of MASLD. Using a female rat dietary model of simple hepatic steatosis without obesity, we confirmed that PemA at 0.5 mg/kg/day was highly effective in reducing liver TG by a mechanism involving a PPARα-related increase in fatty acid catabolism, as we previously reported in the same model using a dose of 1 mg/kg/day [17].

Interestingly, treatment of HFHFr-fed rats with Tel 10 mg/kg/day also caused a reduction in hepatic fat accumulation of similar magnitude as PemA, assessed by ORO/H&E staining of rat liver sections, and by analysis of hepatic TG content. To confirm Tel's efficacy and explore its mechanism, we additionally examined it's anti-steatotic effect in another *in vivo* model of MASLD, using zebrafish larvae. In recent years, zebrafish has emerged as an interesting alternative model that facilitates the study of MASLD physiopathology and treatment evaluation. Zebrafish models are simpler and more economic than rodent models, that show a carbohydrate/lipid metabolism and liver physiology similar to mammals, as well as the ability to develop rapid and progressive MASLD when challenged with the appropriate dietary stimuli [35]. Specifically, 5-dpf zebrafish larvae have a functional liver, are transparent, and more amenable than adults to experiments requiring a large number of individuals to ensure adequate statistical power [36]. To obtain a dietary model of MASLD comparable to the HFHFr rat model, we used overfed 10 dpf larvae that had been exposed to a 3% solution of simple sugars (fructose or glucose) dissolved in the medium. The experiments in zebrafish larvae showed a stronger effect of glucose than fructose on hepatic parameters, characterized by earlier and more intense hepatic fat accumulation, accompanied by an increase in liver size. Although we used fructose in our rat model, a recent report shows that both sugars induce MASLD to the same extent in a similar experimental setting [37]. Hence, we chose glucose to promote hepatic steatosis in zebrafish larvae. Using this model, we confirmed the antisteatotic effect of Tel at a dose of 2 µM, close to the maximal blood concentration of the drug after its oral administration to rats [38].

So far, the positive effects of Tel on liver health in MASH animal models and in humans have been mainly attributed to its antifibrotic, anti-inflammatory, antioxidant and insulin sensitizing properties [14]. In contrast, simple steatosis in the clinical setting is often overlooked and remains untreated, with drug treatments being focused on advanced phases of MASLD. However, simple steatosis is associated to a high cardiovascular mortality, so telmisartan repurposing would be ideal as it is a safe drug that could reduce at the same time the liver lipid burden and cardiovascular risk. In this context, our HFHFr rat model – characterized by isolated hepatic steatosis, without fibrosis or marked alterations in glycemic control [16]- represents a suitable pre-clinical model to explore the therapeutic potential of telmisartan in early-stage MASLD, as well as to characterize its antisteatotic mechanism of action. To this end, we first focused on PPARs, as Tel has been described as a PPARY modulator, acting as a partial agonist [13]. Further, it has been shown to activate PPARα in the liver of high-fat diet-fed obese mice [39]. Our results clearly preclude these mechanisms, as Tel treatment did not increase β-oxidation activity in rat livers and did not modify the expression of any PPARα-target genes studied, either in the rat or in the zebrafish model. In addition, our results also rule out that Tel

acts as a PPARY agonist at the doses used in our study, as the hepatic expression of *ppary* and its target gene *cd36* were not increased in either model. Moreover, the hepatic expression and serum levels of adiponectin remained unaltered. We reason that the lack of Tel's effect as a PPARY agonist in our *in vivo* study could be related to the dose used. Although the dose was chosen on the basis of similar studies [40], Tel activates PPARY at micromolar concentrations, while exhibiting a sub-nanomolar IC50 value toward AGTR1 [41]. Thus, even though after its oral administration Tel accumulates in the liver [39], the concentration reached in this organ may be too low to activate PPARY, while it may suffice to block AGTR1.

Tel's PPARY partial agonist properties have been suggested to pay a role in its ability to attenuate body mass gain and adiposity in rodents fed on a HFD [42–44]. However, the absence of key indicators of PPARY activation suggests that Tel effects may be primarily mediated by AGTR1 blockade, as supported by findings in Agtr1 knockout mice, which also exhibit reduced adiposity [45]. These results, further supports that Tel does not behave as a PPAR modulator in our study.

Several reports suggest that alterations in the RAS may be linked to MASLD [46,47]. Knocking out *Agtr1* in a mouse model of steatohepatitis, as well as silencing the expression of this receptor in HepG2 cells, reduced hepatic lipid accumulation [48]. In accordance with these results, CRISPR/Cas9-induced mutations in *agtr1* in our zebrafish model exerted a protective effect against hepatic steatosis, confirming the involvement of the local hepatic RAS pathways in the accumulation of liver lipids. Two distinct pathways, the classical and the alternative RAS, play a crucial role in liver physiology and pathology. The classical ACE/Ang II/AGTR1 pathway is associated with pro-inflammatory, pro-oxidant, and pro-fibrogenic effects in the liver. In contrast, the alternative RAS ACE2/Ang (1–7)/MasR axis has emerged as a counterbalance to the classical pathway, with ACE2 overexpression improving steatotic liver in *db/db* mice [49] and MasR deletion aggravates steatosis in HFD-fed mice [50]. Here we show that Tel's effects on liver fat and liver size were attenuated in zebrafish larvae with CRISPR/Cas9-induced mutations in *agtr1*. Moreover, Tel treatment reversed the decrease in hepatic ACE2 protein levels caused by the HFHFr diet in rats. However, although upregulation of the alternative pathway has been reported after treatment with ARBs [14], we only detected increased hepatic ACE2 protein levels, while the ang (1-7) serum levels, MasR protein and downstream effectors remained unchanged. Thus, our results suggest that at least part of Tel's antisteatotic effects are driven through the blockade of the AGTR1-mediated detrimental effects, rather than by activation of the alternative RAS pathway. However, we cannot totally rule out the possibility that in the long term a reduction in hepatic ACE2 could potentially influence circulating Ang-(1-7) levels.

The accumulation of hepatic lipids in rats and individuals with MASLD highly depends on increased DNL [16,51]. Therefore, we sought to determine whether Tel modulates expression or protein levels of genes and transcription factors involved in this pathway. Our initial results were not conclusive, because despite the reduced expression of some key enzymes in liver of Tel-treated rats, the magnitude of effect was low compared with the almost complete reversion of liver lipid accumulation caused by this drug. Moreover, the main lipogenic transcription factors ChREBP and SREBP-1c were unaffected. Nevertheless, as Tel reduced the amount of liver TG and associated fatty acids in the absence of i) a decreased food consumption, ii) enhanced fatty acid catabolism and iii) increased TG export from liver to blood, we reasoned that the flux of metabolites directed to hepatic lipid synthesis might be impaired, contributing to reduced accretion of hepatic TG. To explore this possibility,

metabolomics offers advantages over gene or protein expression analysis, because it directly measures the end products of cellular processes and reflects what is currently happening in response to different stimuli, in this case diet and drug treatment. The results of untargeted metabolomic analysis of liver samples showed that Tel treatment restored levels of several key metabolites that had been reduced by the HFHFr diet, like phosphoenolpyruvic acid (PEP). PEP is generated from oxalacetate in the hepatic cytoplasm, via the main gluconeogenic enzyme PCK1. In accordance with metabolomics results, PCK1 protein levels were reduced in HFHFr-fed rat liver [16], consistent with our previous research in rats supplemented with liquid fructose [16,52–54]. Here, we show that PCK1 reduction induced in rats by a HFHFr diet was reversed by Tel treatment, but not by PemA or by the combination of P+T. These results indicate that this is a specific effect of Tel that requires the full dose of this compound (10 mg/kg/day), while in the P+T group we used half the dose of each one. Despite P+T combination did not increase PCK1, it still reduced hepatic steatosis, presumably due to the strong activation of PPARα elicited by PemA, even at very low doses. In zebrafish larvae, the ability of Tel to reduce liver fat content was impaired if *pck1* is perturbed, thereby sustaining the importance of PCK1 regulation in Tel-induced responses.

Interestingly, the amount of phosphoglyceric acid, an intermediate metabolite of the gluconeogenic pathway, was also halved by HFHFr diet and doubled by Tel treatment. On the other hand, the PEP precursor oxalacetate is the product of malic acid oxidation, and malic acid is generated in the mitochondrial Krebs cycle from fumarate and then exported to the cytosol. Levels of these metabolites, and of maleic acid (an isomer of fumaric acid) followed the same pattern: they were significantly lower in HFHFr samples compared with CT, and higher in Tel samples *vs.* HFHFr. These results suggested that gluconeogenesis was favored in rat liver after Tel treatment. However, neither blood glucose, insulin levels, nor hepatic glycogen concentrations were modified, indicating that glucose generated was neither exported to the bloodstream or stored in the liver. Importantly, the levels of sorbitol and fructose, which originate from gluconeogenesis-derived glucose via the polyol pathway, were significantly higher in liver of Tel treated rats. To reconcile these data, we propose the following hypothesis (Fig. 12): in HFHFr fed rats, reduced hepatic PCK1 expression inhibits gluconeogenesis, fueling the metabolic fate of ingested fructose toward lipid synthesis, and contributing to the deposition of TG in the liver. This is in line with the results of Ye et al. [55], who demonstrated reduced hepatic PCK1 expression in mice and humans with MASLD, and showed that PCK1 deficiency in mice stimulated lipid synthesis and deposition in the liver. Our results further suggest that Tel treatment opposes this mechanism by increasing gluconeogenesis and reducing the flux of metabolites into lipogenesis. Glucose synthesized by enhanced gluconeogenesis is diverted to a metabolic death end, the polyol pathway, generating fructose and sorbitol. Since the polyol pathway consumes NADPH and NAD^+, part of the gluconeogenic substrate is also derived to the PPP and to the Purine/Pyrimidine pathways to regenerate the levels of those coenzymes.

Several limitations must be acknowledged, like the accumulation of fructose and sorbitol in the liver resulting from an increased polyol pathway after Tel treatment. This may be regarded as a negative finding, as both compounds may cause detrimental effects in the liver [56,57]. Specifically, the consumption of NADPH in the first step of the polyol pathway by the enzyme aldose reductase, could lead to lower amounts of GSH, which would contribute to oxidative stress. Nevertheless, our metabolomic data show that levels of GSSG and GSH were not modified, suggesting preserved redox homeostasis. Although we cannot discard the possibility that long-term treatment induces undesired effects, the higher levels of spermine and

spermidine in the liver of Tel-treated rats could counteract a potential induction of oxidative stress [58]. Moreover, spermidine promotes beneficial effects in the liver by various mechanisms [59,60]. In any case, our results emphasize the importance of reducing fructose ingestion to prevent development of MASLD, a recommendation already included in the current MASLD management guidelines. On the other hand, a limitation to the generalization of the study is that it did not consider gender/sex issues. Nevertheless, we previously demonstrated that the HFHFr diet did not cause overt hepatic steatosis in male rats [19], therefore we used the female model to assess the antisteatotic effects of the assayed drugs.

One of the strengths of our study is that we showed that administering both compounds together at half the dose of each one is equally effective in reducing accumulation of hepatic fat in our rat model. The nearly complete remission of MASL in all groups could have masked any additional potential benefit from the combination. Our results showed that β-oxidation activity was enhanced in the P+T group to a similar magnitude as in the PemA group, suggesting that this compound has reached maximal efficacy at the dose of 0.25 mg/kg/day. In contrast, PCK1 upregulation, the key component of Tel's antisteatotic mechanism, was not shown in the P+T group. Therefore, we cannot confirm that a synergic additive effect was produced with the combination of both compounds. Nevertheless, combination therapy could offer an advantage in the clinical setting, allowing the use of effective lower doses to attenuate steatosis, thereby reducing the risk of adverse effects.

In summary, we show that both PemA and Tel are effective in preclinical models of hepatic steatosis, by different mechanisms. PemA reduces liver lipids essentially by enhancing fatty acid catabolism through its PPARα agonist properties. Tel exerts its antisteatotic effects via PCK1: increased PCK1 levels lead to a reduced flux of metabolites toward lipogenesis, which along with the reduced expression of enzymes involved in DNL causes a decrease in hepatic lipid accumulation. The use of these compounds in a clinical setting could offer the advantage of simultaneously treating liver pathology and extrahepatic co-morbidities. Thus, the combination of reduced hypertriglyceridemia and blood pressure produced by PemA and Tel administration could contribute to the reduction of CVD burden in MASLD patients.

Ethics Approval

Rat experimental procedures described in this article were conducted in accordance to guidelines established by the Bioethics Committee of the University of Barcelona (Autonomous Government of Catalonia Act Biomedicines 2022, 10, 1517 3 of 19 5/21 July 1995), and were approved by the Animal Experimentation Ethics Committee of the University of Barcelona (approval no. 198/21). Zebrafish procedures were carried out in agreement with Swedish animal welfare laws and were approved by the Ethical Committee for Animal Research of the Swedish Ministry of Agriculture (Dnr 5.8.18-13680/2020). The experiments complied with the WMA Statement on animal use in biomedical research and the EU recommendations (Directive 2010/63/EU) for experimental design and analysis in pharmacology care.

CRediT authorship contribution statement

Roger Bentanachs: Formal analysis; Investigation; Methodology; Visualization; Writing – original draft. **Patricia Ramírez-Carrasco, Bianca Braster, Anastasia Emmanouilidou, Endrina Mujica:** Investigation; Methodology. **Maite Rodrigo-Calvo:** Methodology; Visualization. **Cristina Rodríguez:** Methodology; Funding acquisition; Validation, Writing – review & editing;. **Núria Roglans:** Investigation; Data curation; Methodology; Visualization. **Marcel den Hoed:** Funding acquisition; Methodology; Supervision, Writing – review & editing. **Juan Carlos Laguna, Marta Alegret**: Conceptualization; Funding acquisition; Project administration; Supervision; Writing – review & editing.

Declaration of Competing Interest

The authors declare that they have no known competing financial interests or personal relationships that could have appeared to influence the work reported in this paper.

Acknowledgements

This work was supported by project by the following grants: PID2023-146140OB-I00, funded by MICIU/AEI /10.13039/501100011033 and FEDER, UE; 2021SGR-00345 funded by Generalitat de Catalunya; PI24/0613 funded by ISCIII and FEDER; Swedish Heart-Lung Foundation (20230518), Swedish Research Council (2023-02556), NIH/NIDDK-funded Accelerating Medicines Partnership for Common Metabolic Disorders (5UM1DK105554-5000826-5500002718). Handling and storage of zebrafish imaging data were enabled by resources provided by the National Academic Infrastructure for Supercomputing in Sweden (NAISS), partially funded by the Swedish Research Council through grant agreement no. 2022-06725**.** R.B. is a predoctoral fellow, funded by PREDOCS-UB grant from the University of Barcelona. The authors thank Mr. Pol Sánchez (Interquim SA, Spain) for the kind donation of Tel used in the present study.

Data availability

Data will be made available on request.

References

1. Younossi, Z.M.; Kalligeros, M.; Henry, L. Epidemiology of Metabolic Dysfunction Associated Steatotic Liver Disease. *Clin Mol Hepatol* **2024**, doi:10.3350/cmh.2024.0431.

2. Semova, I.; Biddinger, S.B. Triglycerides in Nonalcoholic Fatty Liver Disease: Guilty Until Proven Innocent. *Trends Pharmacol Sci* **2021**, *42*, 183–190, doi:10.1016/j.tips.2020.12.001.

3. Singh, S.; Allen, A.M.; Wang, Z.; Prokop, L.J.; Murad, M.H.; Loomba, R. Fibrosis Progression in Nonalcoholic Fatty Liver vs Nonalcoholic Steatohepatitis: A Systematic Review and Meta-Analysis of Paired-Biopsy Studies. *Clinical Gastroenterology and Hepatology* **2015**, *13*, 643-654.e9, doi:10.1016/j.cgh.2014.04.014.

4. Targher, G.; Byrne, C.D.; Tilg, H. NAFLD and Increased Risk of Cardiovascular Disease: Clinical Associations, Pathophysiological Mechanisms and Pharmacological Implications. *Gut* **2020**, *69*, 1691–1705, doi:10.1136/gutjnl-2020-320622.

5. Simon, T.G.; Roelstraete, B.; Khalili, H.; Hagström, H.; Ludvigsson, J.F. Mortality in Biopsy-Confirmed Nonalcoholic Fatty Liver Disease: Results from a Nationwide Cohort. *Gut* **2021**, *70*, 1375–1382, doi:10.1136/gutjnl-2020-322786.

6. Mantovani, A.; Csermely, A.; Petracca, G.; Beatrice, G.; Corey, K.E.; Simon, T.G.; Byrne, C.D.; Targher, G. Non-Alcoholic Fatty Liver Disease and Risk of Fatal and Non-Fatal Cardiovascular Events: An Updated Systematic Review and Meta-Analysis. *Lancet Gastroenterol Hepatol* **2021**, *6*, 903–913, doi:10.1016/S2468-1253(21)00308-3.

7. Stols-Gonçalves, D.; Hovingh, G.K.; Nieuwdorp, M.; Holleboom, A.G. NAFLD and Atherosclerosis: Two Sides of the Same Dysmetabolic Coin? *Trends in Endocrinology and Metabolism* **2019**, *30*, 891–902, doi:10.1016/j.tem.2019.08.008.

8. Lonardo, A.; Nascimbeni, F.; Mantovani, A.; Targher, G. Hypertension, Diabetes, Atherosclerosis and NASH: Cause or Consequence? *J Hepatol* **2018**, *68*, 335–352, doi:10.1016/j.jhep.2017.09.021.

9. De Gracia Hahn, D.; Duret, A.; Mann, J.P. An AGTR1 Variant Worsens Nonalcoholic Fatty Liver Disease and the Metabolic Syndrome. *American Journal of Gastroenterology* 2019, *114*, 556–559.

10. Alvarado-Ojeda, Z.A.; Trejo-Moreno, C.; Ferat-Osorio, E.; Méndez-Martínez, M.; Fragoso, G.; Rosas-Salgado, G. Role of Angiotensin II in Non-Alcoholic Steatosis Development. *Arch Med Res* **2024**, *55*, doi:10.1016/j.arcmed.2024.102986.

11. Hirata, T.; Tomita, K.; Kawai, T.; Yokoyama, H.; Shimada, A.; Kikuchi, M.; Hirose, H.; Ebinuma, H.; Irie, J.; Ojiro, K.; et al. Effect of Telmisartan or Losartan for Treatment of Nonalcoholic Fatty Liver Disease: Fatty Liver Protection Trial by Telmisartan or Losartan Study (FANTASY). *Int J Endocrinol* **2013**, *2013*, doi:10.1155/2013/587140.

12. Alam, S.; Kabir, J.; Mustafa, G.; Gupta, U.; Hasan, S.; Alam, A. Effect of Telmisartan on Histological Activity and Fibrosis of Non-Alcoholic Steatohepatitis: A 1-Year Randomized Control Trial. *Saudi Journal of Gastroenterology* **2016**, *22*, 69–76, doi:10.4103/1319-3767.173762.

13. Benson, S.C.; Pershadsingh, H.A.; Ho, C.I.; Chittiboyina, A.; Desai, P.; Pravenec, M.; Qi, N.; Wang, J.; Avery, M.A.; Kurtz, T.W. Identification of Telmisartan as a Unique Angiotensin II Receptor Antagonist with Selective PPARγ-Modulating Activity. *Hypertension* **2004**, *43*, 993–1002, doi:10.1161/01.HYP.0000123072.34629.57.

14. Borém, L.M.A.; Neto, J.F.R.; Brandi, I. V; Lelis, D.F.; Santos, S.H.S. The Role of the Angiotensin II Type I Receptor Blocker Telmisartan in the Treatment of Non-Alcoholic Fatty Liver Disease : A Brief Review. **2018**, 394–405, doi:10.1038/s41440-018-0040-6.

15. Puengel, T.; Tacke, F. Pharmacotherapeutic Options for Metabolic Dysfunction-Associated Steatotic Liver Disease: Where Are We Today? *Expert Opin Pharmacother* 2024, *25*, 1249–1263.

16. Velázquez, A.M.; Bentanachs, R.; Sala-Vila, A.; Lázaro, I.; Rodríguez-Morató, J.; Sánchez, R.M.; Alegret, M.; Roglans, N.; Laguna, J.C. ChREBP-Driven DNL and PNPLA3 Expression Induced by Liquid Fructose Are Essential in the Production of Fatty Liver and Hypertriglyceridemia in a High-Fat Diet-Fed Rat Model. *Mol Nutr Food Res* **2022**, *2101115*, doi:10.1002/mnfr.202101115.

17. Bentanachs, R.; Miró, L.; Sánchez, R.M.; Ramírez-Carrasco, P.; Amat, C.; Alegret, M.; Pérez, A.; Roglans, N.; C., L.J. Pemafibrate Abrogates SLD in a Rat Experimental Dietary Model , Inducing a Shift in Fecal Bile Acids and Microbiota Composition. *Biomedicine & Pharmacotherapy* **2024**, *177*, 117067, doi:10.1016/j.biopha.2024.117067.

18. Iwaki, M.; Kobayashi, T.; Nogami, A.; Ogawa, Y.; Imajo, K.; Sakai, E.; Nakada, Y.; Koyama, S.; Kurihashi, T.; Oza, N.; et al. Pemafibrate for Treating MASLD Complicated by Hypertriglyceridaemia: A Multicentre, Open-Label, Randomised Controlled Trial Study Protocol. *BMJ Open* **2024**, *14*, e088862, doi:10.1136/bmjopen-2024-088862.

19. Bentanachs, R.; Blanco, L.; Montesinos, M.; Sala-Vila, A.; Lázaro, I.; Rodríguez-Morató, J.; Sánchez, R.M.; Laguna, J.C.; Roglans, N.; Alegret, M. Adipose Tissue Protects against Hepatic Steatosis in Male Rats Fed a High-Fat Diet plus Liquid Fructose: Sex-Related Differences. *Nutrients* **2023**, *15*, doi:10.3390/nu15183909.

20. Lazarow, P.B. Assay of Peroxisomal SS-Oxidation of Fatty Acids. *Methods Enzymol* **1981**, *72*, 315–319.

21. Qu, S.; Su, D.; Altomonte, J.; Kamagate, A.; He, J.; Perdomo, G.; Tse, T.; Jiang, Y.; Dong, H.H. PPAR{alpha} Mediates the Hypolipidemic Action of Fibrates by Antagonizing FoxO1. *Am J Physiol Endocrinol Metab* **2007**, *292*, E421–E434, doi:10.1152/ajpendo.00157.2006.

22. Sarkar, D. *Non-Alcoholic Steatohepatitis*; Sarkar, D., Ed.; Methods in Molecular Biology; Springer US: New York, NY, 2022; Vol. 2455; ISBN 978-1-0716-2127-1.

23. Bradford, M.M. A Rapid and Sensitive Method for the Quantitation of Microgram Quantities of Protein Utilizing the Principle of Protein-Dye Binding. *Anal. Biochem* **1976**, *72*, 248–254.

24. Her, G.M.; Yeh, Y.H.; Wu, J.L. 435-Bp Liver Regulatory Sequence in the Liver Fatty Acid Binding Protein (L-FABP) Gene Is Sufficient to Modulate Liver Regional Expression in Transgenic Zebrafish. *Developmental Dynamics* **2003**, *227*, 347–356, doi:10.1002/dvdy.10324.

25. Her, G.M.; Chiang, C.C.; Chen, W.Y.; Wu, J.L. In Vivo Studies of Liver-Type Fatty Acid Binding Protein (L-FABP) Gene Expression in Liver of Transgenic Zebrafish (Danio Rerio). *FEBS Lett* **2003**, *538*, 125–133, doi:10.1016/S0014-5793(03)00157-1.

26. Concordet, J.P.; Haeussler, M. CRISPOR: Intuitive Guide Selection for CRISPR/Cas9 Genome Editing Experiments and Screens. *Nucleic Acids Res* **2018**, *46*, W242–W245, doi:10.1093/nar/gky354.

27. Mazzaferro, E.; Mujica, E.; Zhang, H.; Emmanouilidou, A.; Jenseit, A.; Evcimen, B.; Metzendorf, C.; Dethlefsen, O.; Loos, R.J.F.; Vienberg, S.G.; et al. Functionally Characterizing Obesity-Susceptibility Genes Using CRISPR/Cas9, in Vivo Imaging and Deep Learning. *Sci Rep* **2025**, *15*, doi:10.1038/s41598-025-89823-2.

28. Ma, Q.X.; Zhu, W.Y.; Lu, X.C.; Jiang, D.; Xu, F.; Li, J.T.; Zhang, L.; Wu, Y.L.; Chen, Z.J.; Yin, M.; et al. BCAA–BCKA Axis Regulates WAT Browning through Acetylation of PRDM16. *Nat Metab* **2022**, *4*, 106–122, doi:10.1038/s42255-021-00520-6.

29. Song, L.N.; Liu, J.Y.; Shi, T.T.; Zhang, Y.C.; Xin, Z.; Cao, X.; Yang, J.K. Angiotensin-(1-7), the Product of ACE2 Ameliorates NAFLD by Acting through Its Receptor Mas to Regulate Hepatic Mitochondrial Function and Glycolipid Metabolism. *FASEB Journal* **2020**, *34*, 16291–16306, doi:10.1096/fj.202001639R.

30. Jiang, W.; Wang, S.; Xiao, M.; Lin, Y.; Zhou, L.; Lei, Q.; Xiong, Y.; Guan, K.L.; Zhao, S. Acetylation Regulates Gluconeogenesis by Promoting PEPCK1 Degradation via Recruiting the UBR5 Ubiquitin Ligase. *Mol Cell* **2011**, *43*, 33–44, doi:10.1016/j.molcel.2011.04.028.

31. Latorre-Muro, P.; Baeza, J.; Armstrong, E.A.; Hurtado-Guerrero, R.; Corzana, F.; Wu, L.E.; Sinclair, D.A.; López-Buesa, P.; Carrodeguas, J.A.; Denu, J.M. Dynamic Acetylation of Phosphoenolpyruvate Carboxykinase Toggles Enzyme Activity between Gluconeogenic and Anaplerotic Reactions. *Mol Cell* **2018**, *71*, 718-732.e9, doi:10.1016/j.molcel.2018.07.031.

32. Harrison, S.A.; Bedossa, P.; Guy, C.D.; Schattenberg, J.M.; Loomba, R.; Taub, R.; Labriola, D.; Moussa, S.E.; Neff, G.W.; Rinella, M.E.; et al. A Phase 3, Randomized, Controlled Trial of Resmetirom in NASH with Liver Fibrosis. *New England Journal of Medicine* **2024**, *390*, 497–509, doi:10.1056/nejmoa2309000.

33. Powell, E.E. A New Treatment and Updated Clinical Practice Guidelines for MASLD. *Nat Rev Gastroenterol Hepatol* 2024.

34. Ciardullo, S.; Muraca, E.; Vergani, M.; Invernizzi, P.; Perseghin, G. Advancements in Pharmacological Treatment of NAFLD/MASLD: A Focus on Metabolic and Liver-Targeted Interventions. *Gastroenterol Rep (Oxf)* 2024, *12*.

35. Chang, C.; Li, H.; Zhang, R. Zebrafish Facilitate Non-Alcoholic Fatty Liver Disease Research: Tools, Models and Applications. *Liver International* 2023, *43*, 1385–1398.

36. Mujica, E.; den Hoed, M. Investigating the Role of Lipid Genes in Liver Disease Using Models of Steatotic Liver Disease in Zebrafish (Danio Rerio). *Liver International* 2023, *43*, 2348–2350.

37. Hsu, W.F.; Lee, M.H.; Lii, C.K.; Peng, C.Y. No Difference in Liver Damage Induced by Isocaloric Fructose or Glucose in Mice with a High-Fat Diet. *Nutrients* **2024**, *16*, doi:10.3390/nu16203571.

38. Hao, K.; Chen, Y.C.; Cao, Y.G.; Yu, D.; Liu, X.Q.; Wang, G.J. Pharmacokinetic-Pharmacodynamic Modeling of Telmisartan Using an Indirect Response Model in Spontaneously Hypertensive Rats. *Acta Pharmacol Sin* **2007**, *28*, 738–743, doi:10.1111/j.1745-7254.2007.00556.x.

39. Clemenz, M.; Frost, N.; Schupp, M.; Caron, S.; Foryst-Ludwig, A.; Bohm, C.; Hartge, M.; Gust, R.; Staels, B.; Unger, T.; et al. Liver-Specific Peroxisome Proliferator-Activated Receptor α Target Gene Regulation by the Angiotensin Type 1 Receptor Blocker Telmisartan. *Diabetes* **2008**, *57*, 1405–1413, doi:10.2337/db07-0839.

40. Alqarni, I.; Bassiouni, Y.A.; Badr, A.M.; Ali, R.A. Telmisartan and/or Chlorogenic Acid Attenuates Fructose-Induced Non-Alcoholic Fatty Liver Disease in Rats: Implications of Cross-Talk between Angiotensin, the Sphingosine Kinase/Sphingoine-1-Phosphate Pathway, and TLR4 Receptors. *Biochem Pharmacol* **2019**, *164*, 252–262, doi:10.1016/j.bcp.2019.04.018.

41. Lillich, F.F.; Imig, J.D.; Proschak, E. Multi-Target Approaches in Metabolic Syndrome. *Front Pharmacol* 2021, *11*.

42. Rong, X.; Li, Y.; Ebihara, K.; Zhao, M.; Naowaboot, J.; Kusakabe, T.; Kuwahara, K.; Murray, M.; Nakao, K. Angiotensin II Type 1 Receptor-Independent Beneficial Effects of Telmisartan on Dietary-Induced Obesity, Insulin Resistance and Fatty Liver in Mice. *Diabetologia* **2010**, *53*, 1727–1731, doi:10.1007/s00125-010-1744-6.

43. Ayza, M.A.; Zewdie, K.A.; Tesfaye, B.A.; Tesfamariam, S.; Gebrekirstos; Berhe, D.F. Anti-Diabetic Effect of Telmisartan through Its Partial Pparγ-Agonistic Activity. *Diabetes, Metabolic Syndrome and Obesity* 2020, *13*, 3627–3635.

44. Sugimoto, K.; Qi, N.R.; Kazdová, L.; Pravenec, M.; Ogihara, T.; Kurtz, T.W. Telmisartan but Not Valsartan Increases Caloric Expenditure and Protects against Weight Gain and Hepatic Steatosis. *Hypertension* **2006**, *47*, 1003–1009, doi:10.1161/01.HYP.0000215181.60228.f7.

45. Kouyama, R.; Suganami, T.; Nishida, J.; Tanaka, M.; Toyoda, T.; Kiso, M.; Chiwata, T.; Miyamoto, Y.; Yoshimasa, Y.; Fukamizu, A.; et al. Attenuation of Diet-Induced Weight Gain and Adiposity through Increased Energy Expenditure in Mice Lacking Angiotensin II Type 1a Receptor. *Endocrinology* **2005**, *146*, 3481–3489, doi:10.1210/en.2005-0003.

46. Wu, Y.; Ma, K.L.; Zhang, Y.; Wen, Y.; Wang, G.H.; Hu, Z.B.; Liu, L.; Lu, J.; Chen, P.P.; Ruan, X.Z.; et al. Lipid Disorder and Intrahepatic Renin–Angiotensin System Activation Synergistically Contribute to Non-Alcoholic Fatty Liver Disease. *Liver International* **2016**, *36*, 1525–1534, doi:10.1111/liv.13131.

47. Mastoor, Z.; Diz-Chaves, Y.; González-Matías, L.C.; Mallo, F. Renin–Angiotensin System in Liver Metabolism: Gender Differences and Role of Incretins. *Metabolites* 2022, *12*.

48. Nabeshima, Y.; Tazuma, S.; Kanno, K.; Hyogo, H.; Chayama, K. Deletion of Angiotensin II Type I Receptor Reduces Hepatic Steatosis. *J Hepatol* **2009**, *50*, 1226–1235, doi:10.1016/j.jhep.2009.01.018.

49. Cao, X.; Yang, F.; Shi, T.; Yuan, M.; Xin, Z.; Xie, R.; Li, S.; Li, H.; Yang, J.K. Angiotensin-Converting Enzyme 2/Angiotensin-(1-7)/Mas Axis Activates Akt Signaling to Ameliorate Hepatic Steatosis. *Sci Rep* **2016**, *6*, doi:10.1038/srep21592.

50. Song, L.N.; Liu, J.Y.; Shi, T.T.; Zhang, Y.C.; Xin, Z.; Cao, X.; Yang, J.K. Angiotensin-(1-7), the Product of ACE2 Ameliorates NAFLD by Acting through Its Receptor Mas to Regulate Hepatic Mitochondrial Function and Glycolipid Metabolism. *FASEB Journal* **2020**, *34*, 16291–16306, doi:10.1096/fj.202001639R.

51. Chakravarthy, M. V.; Waddell, T.; Banerjee, R.; Guess, N. Nutrition and Nonalcoholic Fatty Liver Disease: Current Perspectives. *Gastroenterol Clin North Am* **2020**, *49*, 63–94, doi:10.1016/j.gtc.2019.09.003.

52. Rebollo, A.; Roglans, N.; Baena, M.; Padrosa, A.; Sanchez, R.M.; Merlos, M.; Alegret, M.; Laguna, J.C. Liquid Fructose Down-Regulates Liver Insulin Receptor Substrate 2 and Gluconeogenic Enzymes by Modifying Nutrient Sensing Factors in Rats. *J Nutr Biochem* **2014**, *25*, 250–258, doi:10.1016/j.jnutbio.2013.10.014.

53. Baena, M.; Sangüesa, G.; Dávalos, A.; Latasa, M.-J.M.-J.J.; Sala-Vila, A.; Sánchez, R.M.R.M.; Roglans, N.; Laguna, J.C.J.C.; Alegret, M.; Sanguesa, G.; et al. Fructose, but Not Glucose, Impairs Insulin Signaling in the Three Major Insulin-Sensitive Tissues. *Sci Rep* **2016**, *6*, 26149, doi:10.1038/srep26149.

54. Sangüesa, G.; Montañés, J.C.; Baena, M.; Sánchez, R.M.; Roglans, N.; Alegret, M.; Laguna, J.C. Chronic Fructose Intake Does Not Induce Liver Steatosis and Inflammation in Female Sprague–Dawley Rats, but Causes Hypertriglyceridemia Related to Decreased VLDL Receptor Expression. *Eur J Nutr* **2018**, doi:10.1007/s00394-018-1654-9.

55. Ye, Q.; Liu, Y.; Zhang, G.; Deng, H.; Wang, X.; Tuo, L.; Chen, C.; Pan, X.; Wu, K.; Fan, J.; et al. Deficiency of Gluconeogenic Enzyme PCK1 Promotes Metabolic-Associated Fatty Liver Disease through PI3K/AKT/PDGF Axis Activation in Male Mice. *Nat Commun* **2023**, *14*, doi:10.1038/s41467-023-37142-3.

56. Gallagher, E.J.; LeRoith, D.; Stasinopoulos, M.; Zelenko, Z.; Shiloach, J. Polyol Accumulation in Muscle and Liver in a Mouse Model of Type 2 Diabetes. *J Diabetes Complications* **2016**, *30*, 999–1007, doi:10.1016/j.jdiacomp.2016.04.019.

57. Lanaspa, M. a; Ishimoto, T.; Li, N.; Cicerchi, C.; Orlicky, D.J.; Ruzicky, P.; Rivard, C.; Inaba, S.; Roncal-Jimenez, C. a; Bales, E.S.; et al. Endogenous Fructose Production and Metabolism in the Liver Contributes to the Development of Metabolic Syndrome. *Nat Commun* **2013**, *4*, 2434, doi:10.1038/ncomms3434.

58. Rider, J.E.; Hacker, A.; Mackintosh, C.A.; Pegg, A.E.; Woster, P.M.; Casero, R.A. Spermine and Spermidine Mediate Protection against Oxidative Damage Caused by Hydrogen Peroxide. *Amino Acids* **2007**, *33*, 231–240, doi:10.1007/s00726-007-0513-4.

59. Yue, F.; Li, W.; Zou, J.; Jiang, X.; Xu, G.; Huang, H.; Liu, L. Spermidine Prolongs Lifespan and Prevents Liver Fibrosis and Hepatocellular Carcinoma by Activating MAP1S-Mediated Autophagy. *Cancer Res* **2017**, *77*, 2938–2951, doi:10.1158/0008-5472.CAN-16-3462.

60. Madeo, F.; Eisenberg, T.; Pietrocola, F.; Kroemer, G. Spermidine in Health and Disease. *Science (1979)* 2018, *359*.

Figure legends

Fig. 1. Drug treatment does not alter energy consumption, body weight circulating lipids or glucose levels. A) Total calorie intake, expressed as area under the curve (AUC) in Kcal/cage/90 days. B) Final body weight. Blood/serum concentrations of cholesterol (C), TG (D), glucose (E), insulin (F), ISI (G). Quantitative results are presented as bar plots with individual values, showing the mean ± SD of 6–8 animals/group. * P<0.05, ***P<0.001.

Fig. 2. Treatment with PemA, Tel and their combination reduces the NAFLD activity score (NAS). Representative images of Oil Red O-stained (A) and Hematoxylin-Eosin (B) stained and Sirius Red (C) sections of liver samples along with the corresponding histological analysis from CT, HFHFr, PemA, Tel and P+T. (D) shows NAFLD activity score, and (E) the subcomponent scores. AST (F), ALT (G), and (H) relative mRNA levels of markers of inflammation/oxidative stress fibrosis. Absolute (I) and relative (J) liver weight. Hepatic content of cholesterol (K) and TG (L). Quantitative results are presented as bar plots with individual values, showing the mean ± SD of 6–8 animals/group. * P<0.05, ** P<0.01, ***P<0.001 ****P<0.0001.

Fig. 3. Treatment with PemA increased hepatic fatty acid oxidation. (A) Fatty acid β-oxidation activity and (B) mRNA levels of genes related to fatty acid catabolism. Serum FGF21 (C) and ANGTL3 (E) levels from all experimental groups. (D) Relative content of KHK protein levels in liver samples, along with the representative Western Blot bands from HFHFr, PemA, Tel and P+T groups. Quantitative results are presented as bar plots with individual values, showing the mean ± SD of 6–8 animals/group. * P<0.05, ** P<0.01, ***P<0.001 ****P<0.0001.

Fig. 4. The antisteatotic effect of telmisartan is PPARγ-independent. Relative mRNA levels of PPARγ target genes in liver (A) and pWAT (B) from CT, HFHFr and Tel groups. (C) Serum adiponectin levels, (D) relative weights of BAT, pWAT and sWAT and (E) serum NEFA concentrations in CT, HFHFr and Tel groups. (F) Relative mRNA levels of browning markers in pWAT from CT, HFHFr and Tel groups. (G) UCP1 protein levels in pWAT from HFHFr and Tel groups. On the upper part of the figure, representative western blot bands corresponding to the mentioned groups. Quantitative results are presented as bar plots with individual values, showing the mean ± SD of 6–8 animals/group. * P<0.05

Fig. 5. Effects of telmisartan treatment on the renin angiotensin system. (A) Relative liver ace2 and agtr1 mRNA levels in the livers of CT, HFHFr and CT groups. (B) Relative liver protein levels of ACE2 and AGTR1 from CT and HFHFr groups. (C) Relative liver protein levels of ACE2, AGTR1, phosphor/total AMPK and phosphor/total AKT from HFHFr and Tel groups. On the right part of the figures C and D, representative western blot bands corresponding to the mentioned groups. Serum ang (1-7) and MasR liver protein levels from CT, HFHFr and Tel groups.

Quantitative results are presented as bar plots with individual values, showing the mean ± SD of 6–8 animals/group. * P<0.05.

Fig. 6. Effects of telmisartan treatment on key enzymes involved in de novo lipogenesis (DNL). Relative mRNA (A) and protein levels (B) of liver DNL markers. On the right part of the figure, representative western blot bands corresponding to HFHFr and Tel groups are shown. Quantitative results are presented as bar plots with individual values, showing the mean ± SD of 6–8 animals/group. * P<0.05.

Fig. 7. Metabolomic analysis of liver samples from CT, HFHFr Tel groups. Principal component analysis (A) and partial least squares discriminant analysis (B) showing the clustering patterns and separation of metabolic profiles from the different groups. Volcano plots highlighting significant differences ($p < 0.05$, $|Log_2FC| > 0.5$, colored) in CT vs HFHFr (C) and Tel vs. HFHFr (D). Pathway enrichment analysis using Over-Representation Analysis with metabolites that were significantly altered (differences ($p < 0.05$, $|Log_2FC| > 0.5$) in the CT vs. HFHFr (E) and HFHFr vs. Tel (F) comparisons. Dot size is proportional to the number of hits per pathway.

Fig. 8. Relevant liver metabolites involved in the antisteatotic effect of telmisartan. Box plots showing the levels of metabolites involved in gluconeogenesis and polyol pathways (A), and those related to pentose phosphate pathway and purine/pyrimidine metabolism (B). Metabolite signal intensities were Z-score normalized for plotting purposes. Statistical analysis was performed with raw data from 6-8 animals per group. * P<0.05. ** P<0.01, ***P<0.001 ****P<0.0001.

Fig. 9. Telmisartan effects on PCK1 expression. (A) Relative liver mRNA levels of pck1 and ubr5 from CT, HFHF rand Tel groups. (B, C) Relative liver protein levels of PCK1, p-GSK3β and SIRT1 from the corresponding experimental groups. On the upper part of the figures, representative western blot bands are shown. (D) Ubiquitinated PCK1 protein levels relative to total PCK1 protein levels in the livers from CT, HFHFr and Tel groups. (E) Hepatic glycogen content from CT, HFHFr and Tel groups. Quantitative results are presented as bar plots with individual values, showing the mean ± SD of 6–8 animals/group. * P<0.05, ** P<0.01.

Fig. 10. Telmisartan effects on OF+GL model. (A) Schematic representation of the experimental design. (B) Scatter plot of the normalized (Z-score) Liver Lipid Area and Liver Area individual values along with margin plots in the SF, OF+GL and Tel at different concentrations. Scatter plot, mean and standard deviation of the survival rate (%) in experimental tanks from 8 to 10 days post fertilization from CT, OF+GL, Tel 0.4µM and Tel 2µM groups. (C) Length, Dorsal Area and Lateral Area of SF, Tel 0.4µM or Tel 2µM vs OF+GL group. Analysis was performed using multiple linear regression adjusting the values by “Time of day” and “Batch” (3 Batches). Dorsal and lateral area were additionally adjusted by length. Fold change calculated using raw data is indicated when the differences are statistically significant (p<0,05) between indicated groups.

Fig. 11. Evaluation of the effects of agtr1 or pck1 mutations, telmisartan treatment or both in OF+GL fed larvae. (A) Schematic representation of the experimental design. Scatter plot of the inversely normalized Liver Lipid Area and Liver Area individual values, along with margin plots for the untreated and treated Controls as well as for their respective untreated and treated agtr1 (B) or pck1 (C) mutant siblings. Box plots showing the survival rate (%) in Telmisartan 2µM treated or untreated experimental tanks from 8 to 10 days post fertilization. (D) Effect of mutations and telmisartan treatment or both on Length, Dorsal and Lateral area. Analysis was performed using multiple linear regression adjusting the values by “Time of day” and “Batch” (2 Batches). Fold change calculated using raw data is indicated when the differences are statistically significant ($p<0,05$) between groups differing by a single variable.

Fig. 12. Telmisartan proposed mechanism of action. Blue arrows correspond to the direction of the metabolic flux following telmisartan treatment. Grey and blue sings next to the metabolites indicate the metabolomic analysis results for the HFHFr and Tel groups respectively. DHAP: dihydroxyacetone phosphate; F-1-p: fructose 1-phosphate; F-1,6-p: fructose 1,6-diphosphate; F-6-p: fructose 6-phosphate; G-6-p: glucose 6-phosphate; GA3P: glyceraldehyde 3-phosphateGSH: reduced glutathione; GSSG: oxidized glutathione; OAA: oxalacetate; PRPP: phosphoribosyl pyrophosphate.

Graphical Abstract

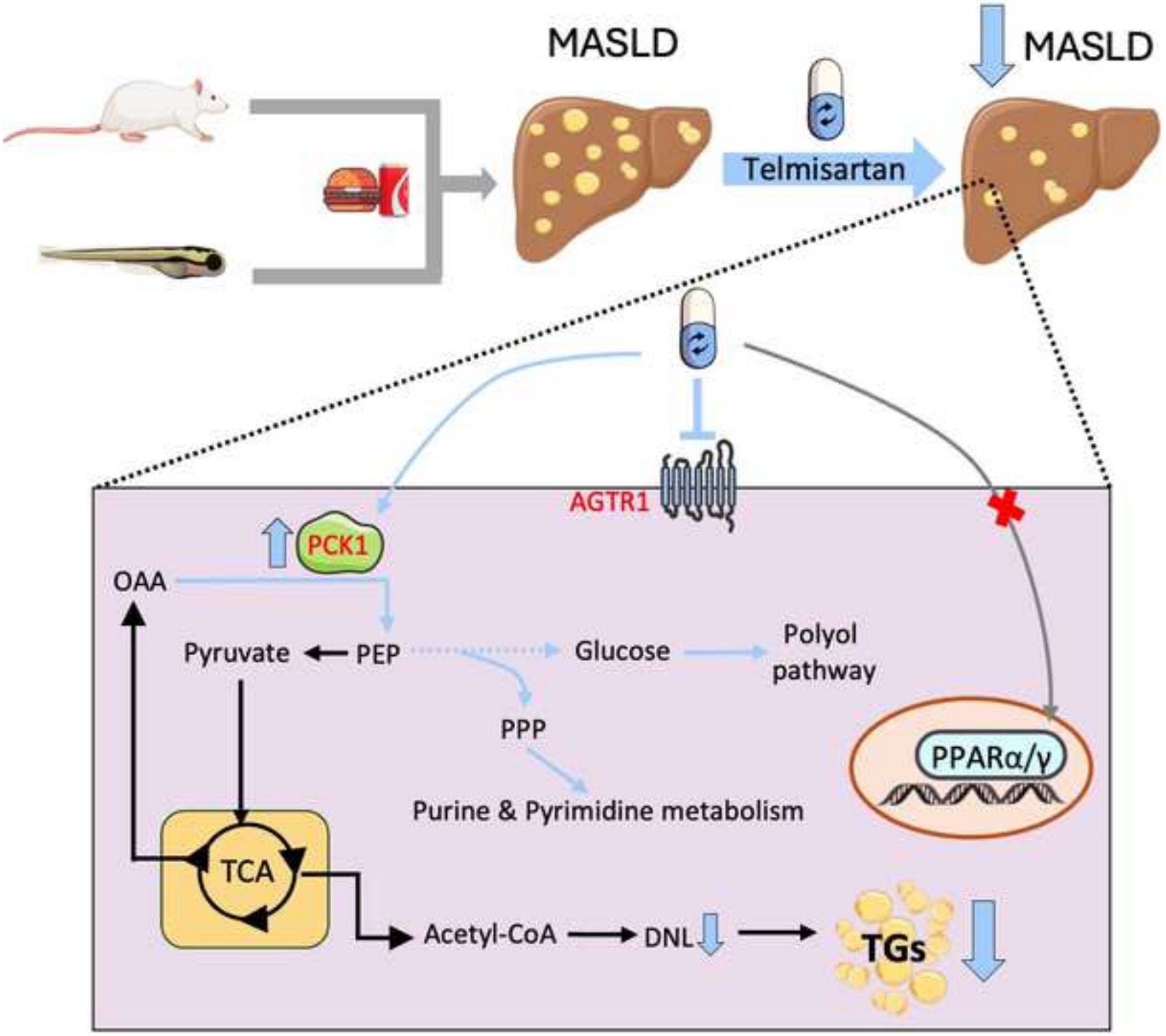

Figure 1

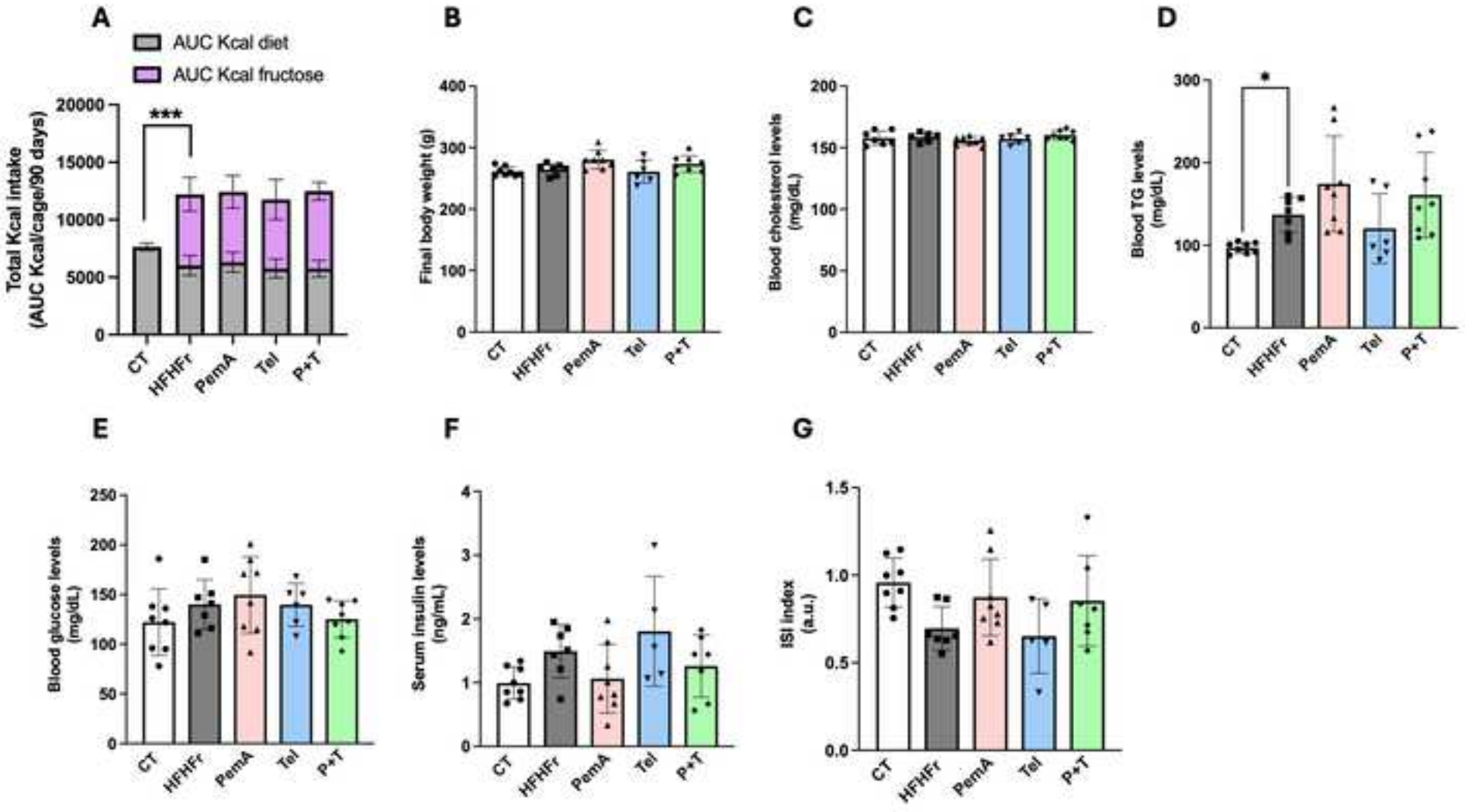

Figure 2

Click here to access/download;Figure;Fig2_Sirius.jpg

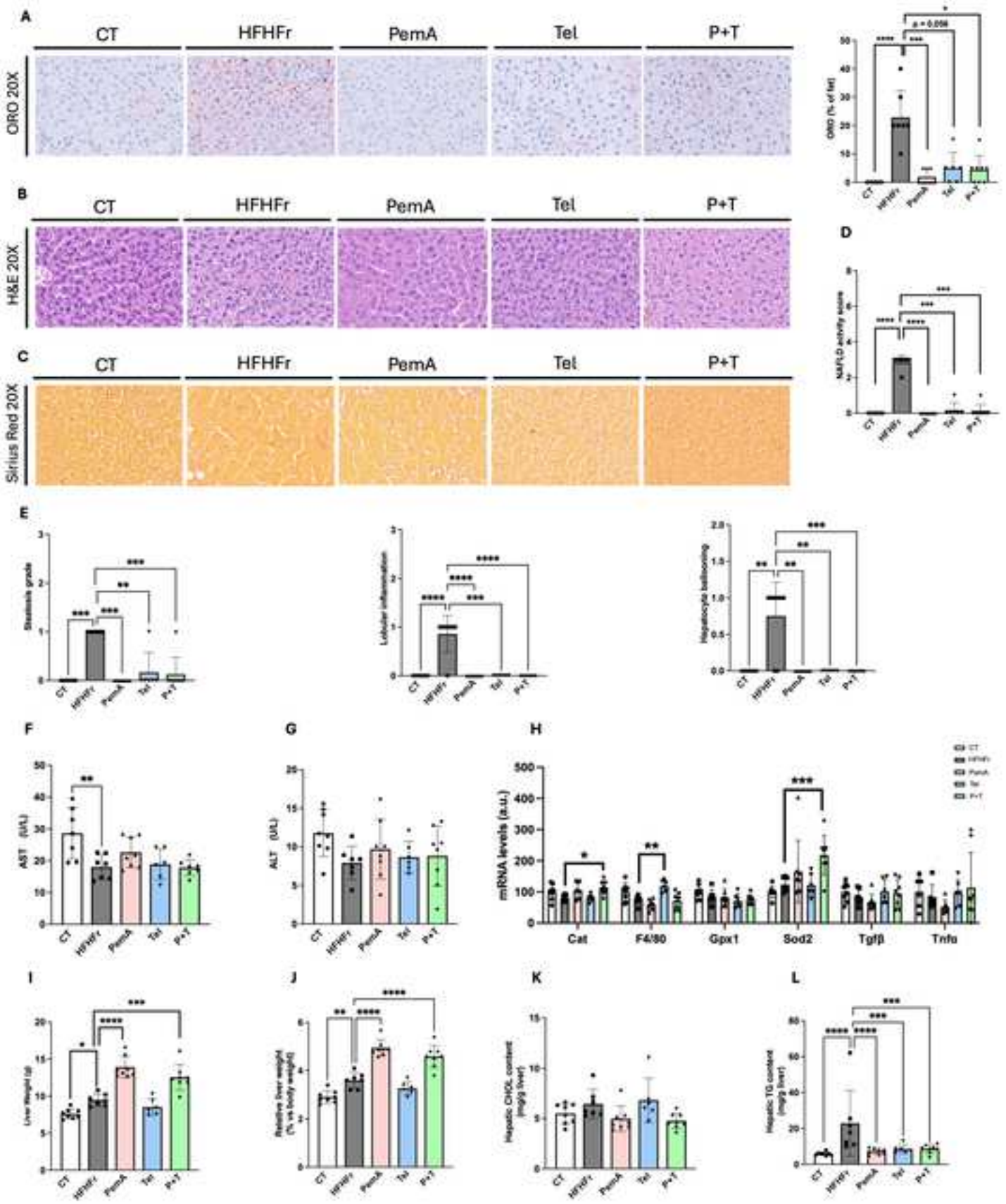

Figure 3

Click here to access/download;Figure;Fig3.jpg

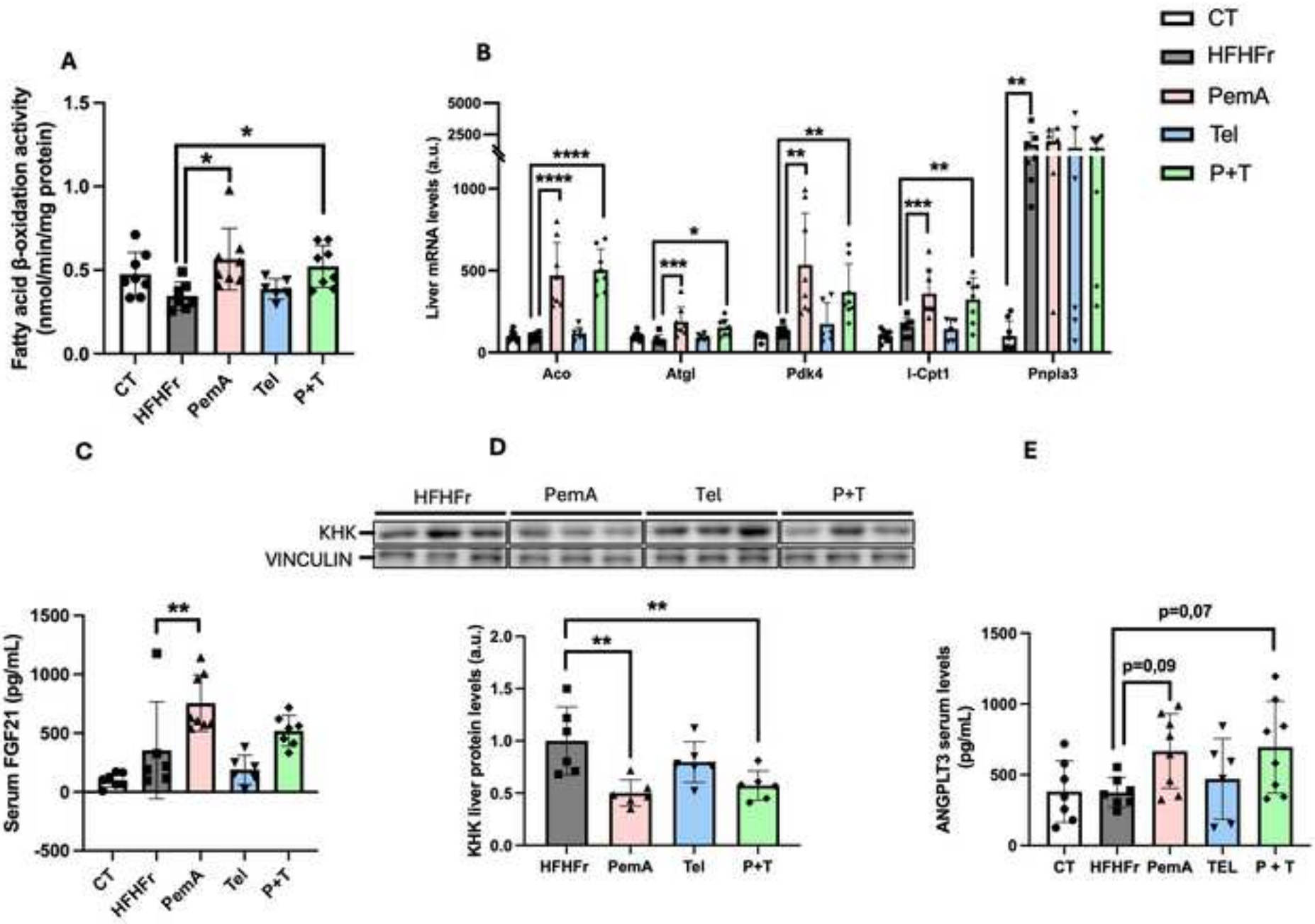

Figure 4

Click here to access/download;Figure;Fig4.jpg

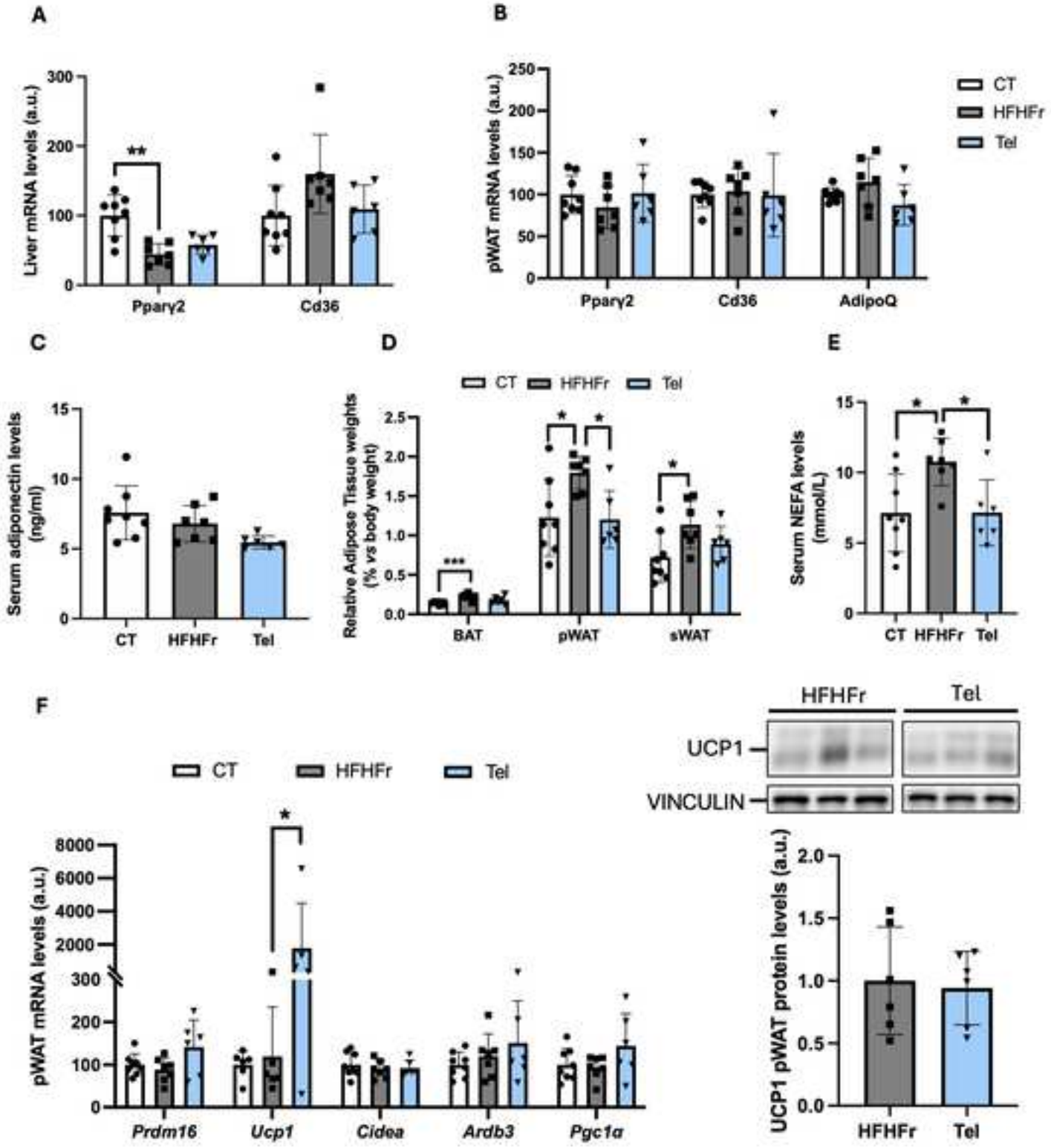

Figure 5

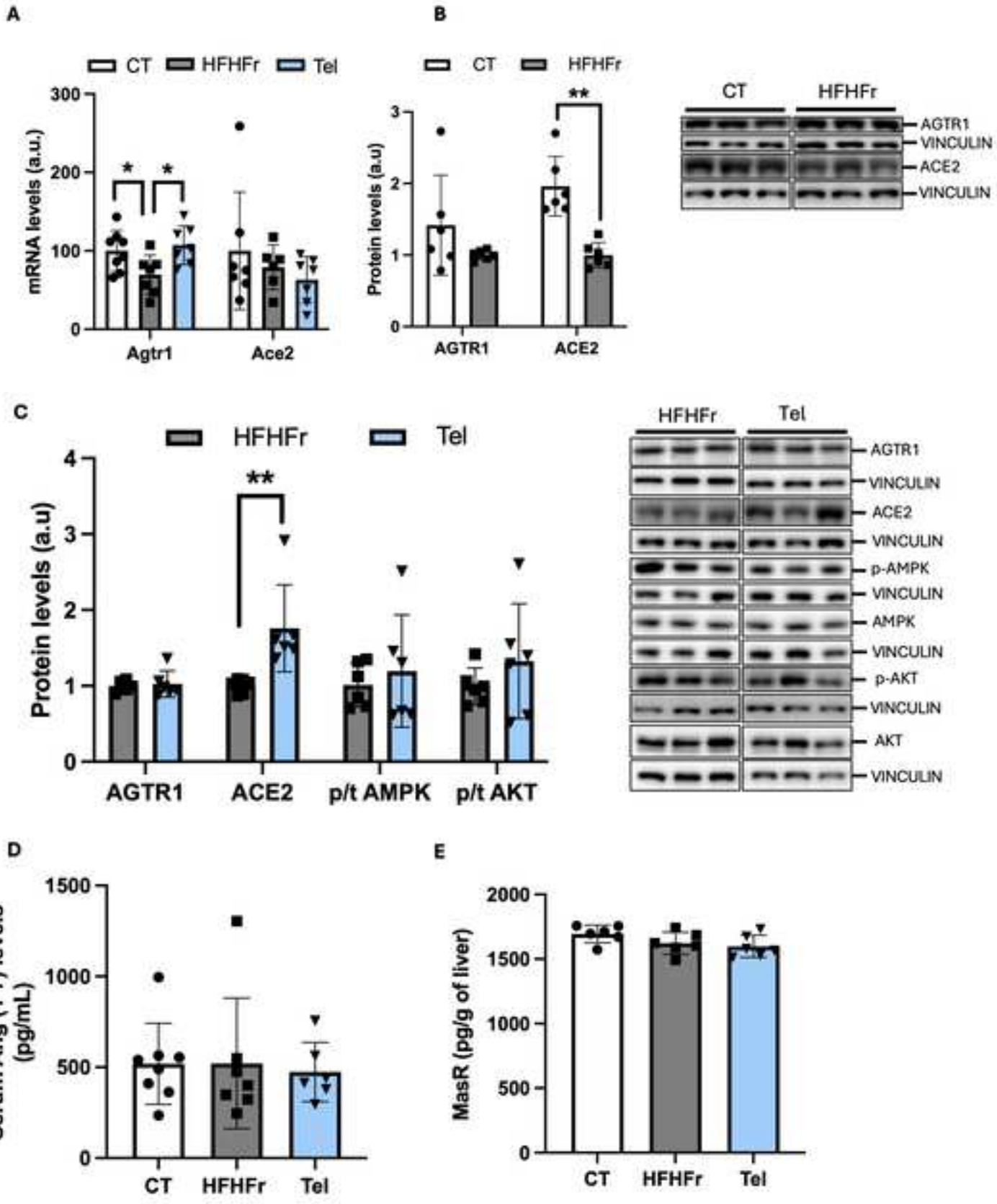

Figure 6

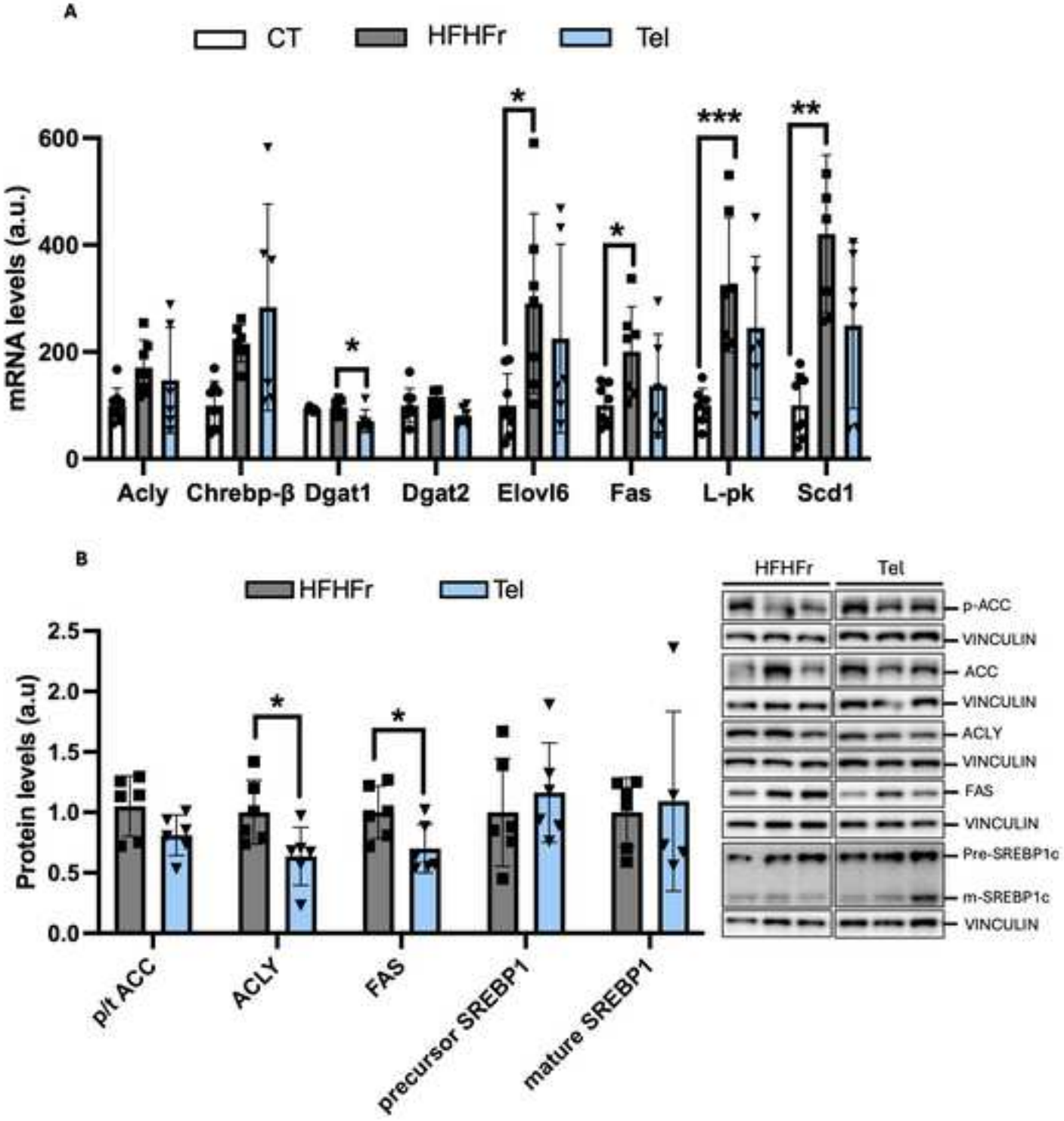

Figure 7

Click here to access/download;Figure;Fig7.jpg

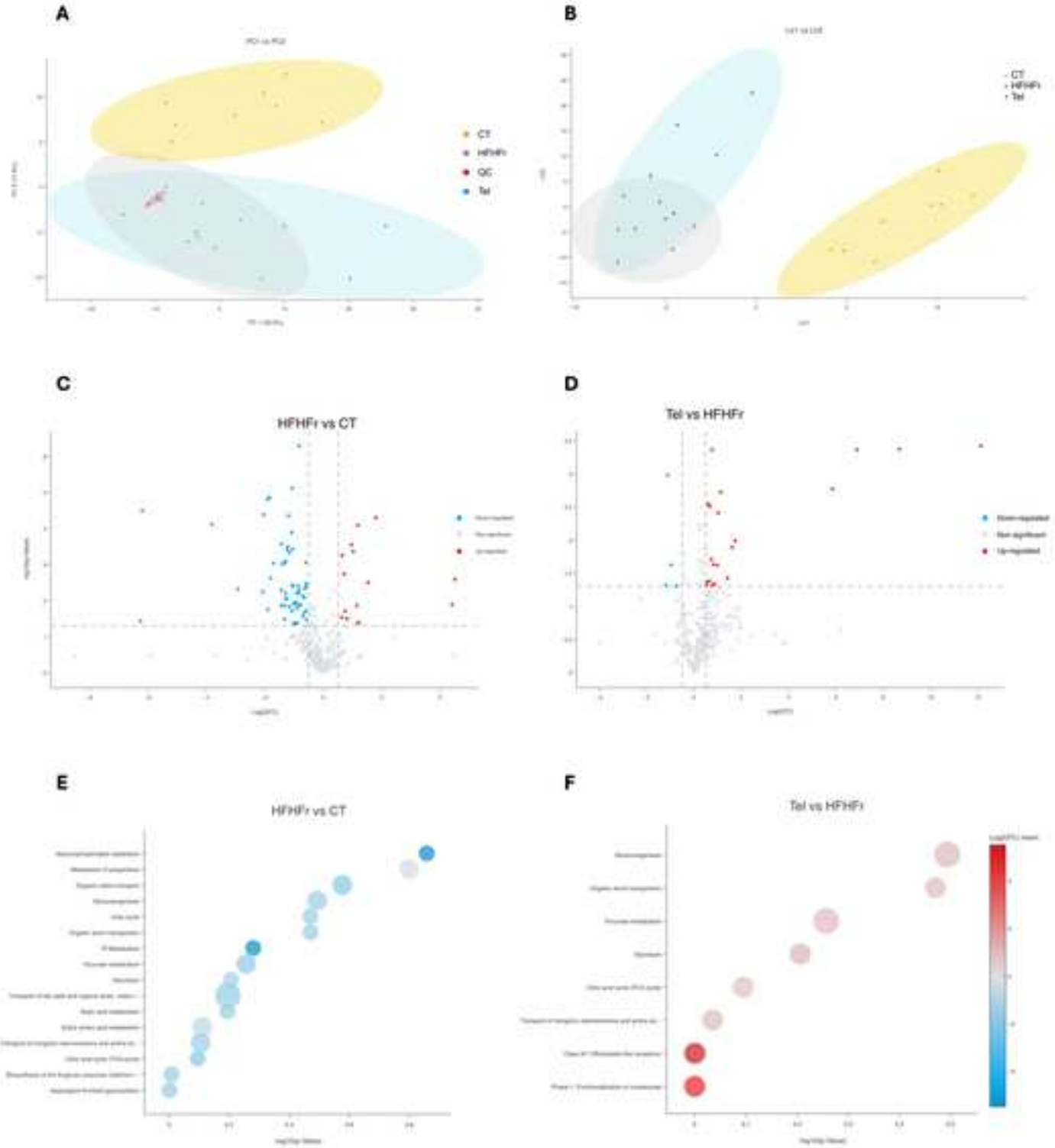

Figure 8

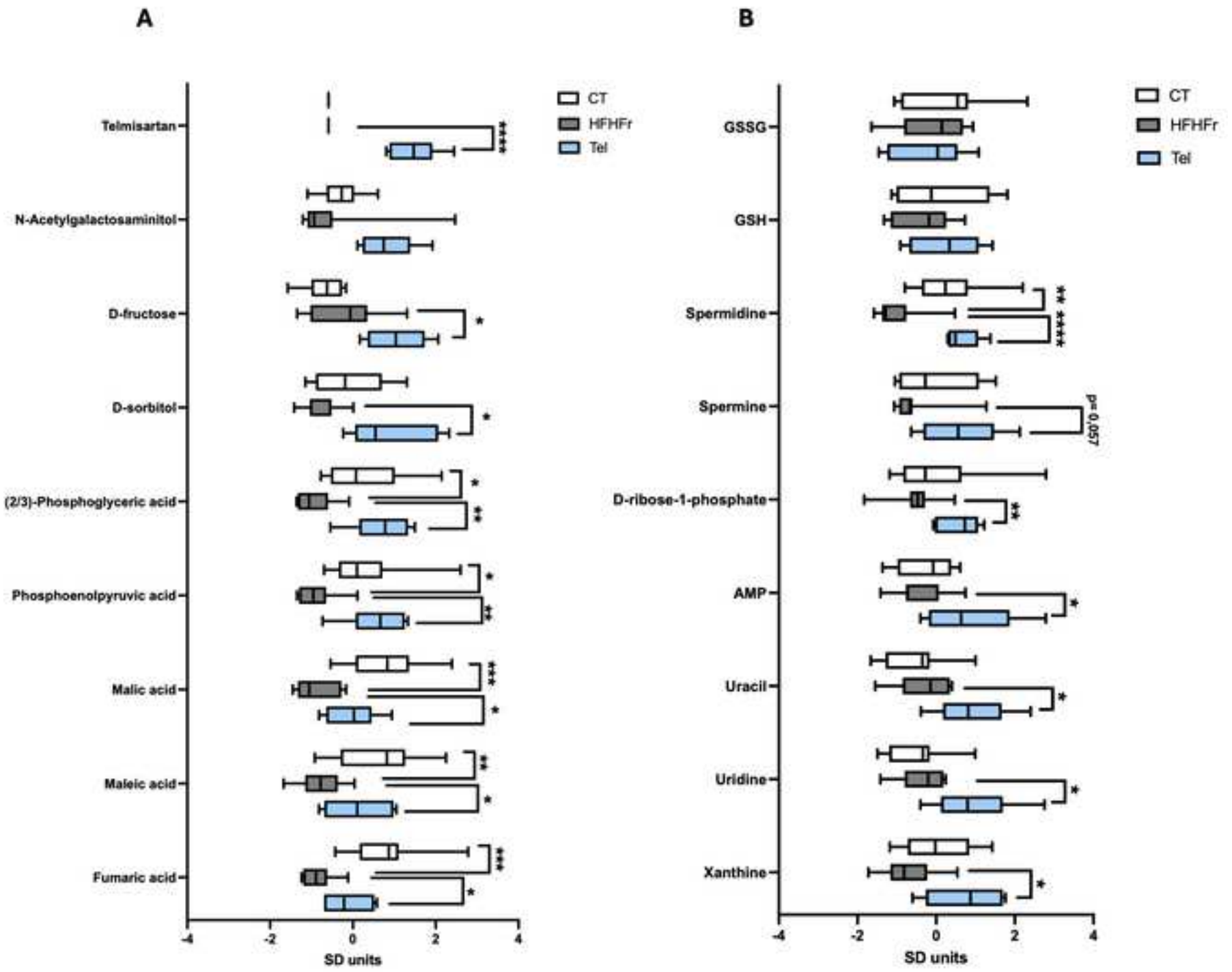

Figure 9

Click here to access/download;Figure;Fig9.jpg

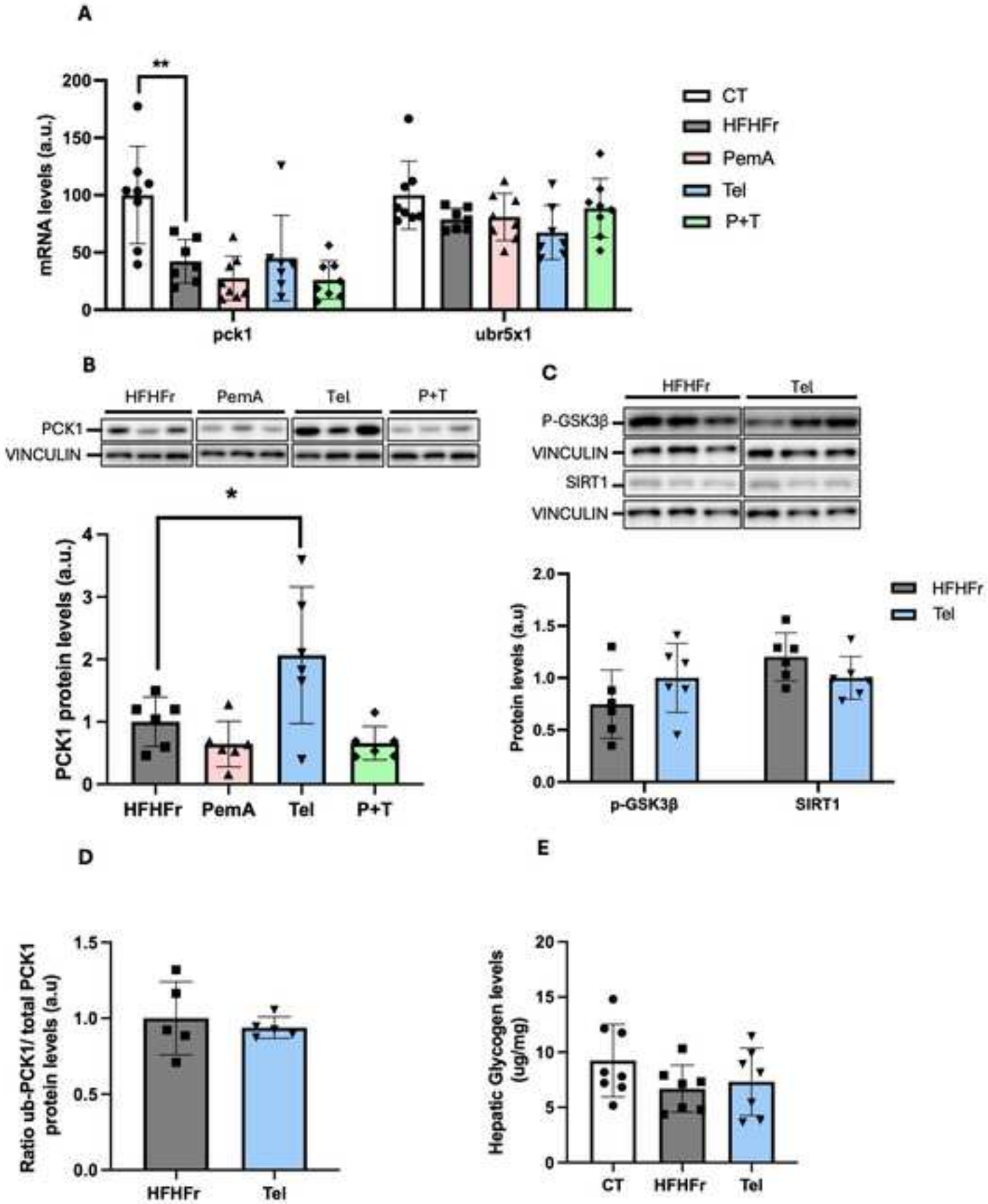

Figure 10

Click here to access/download;Figure;Fig10.jpg

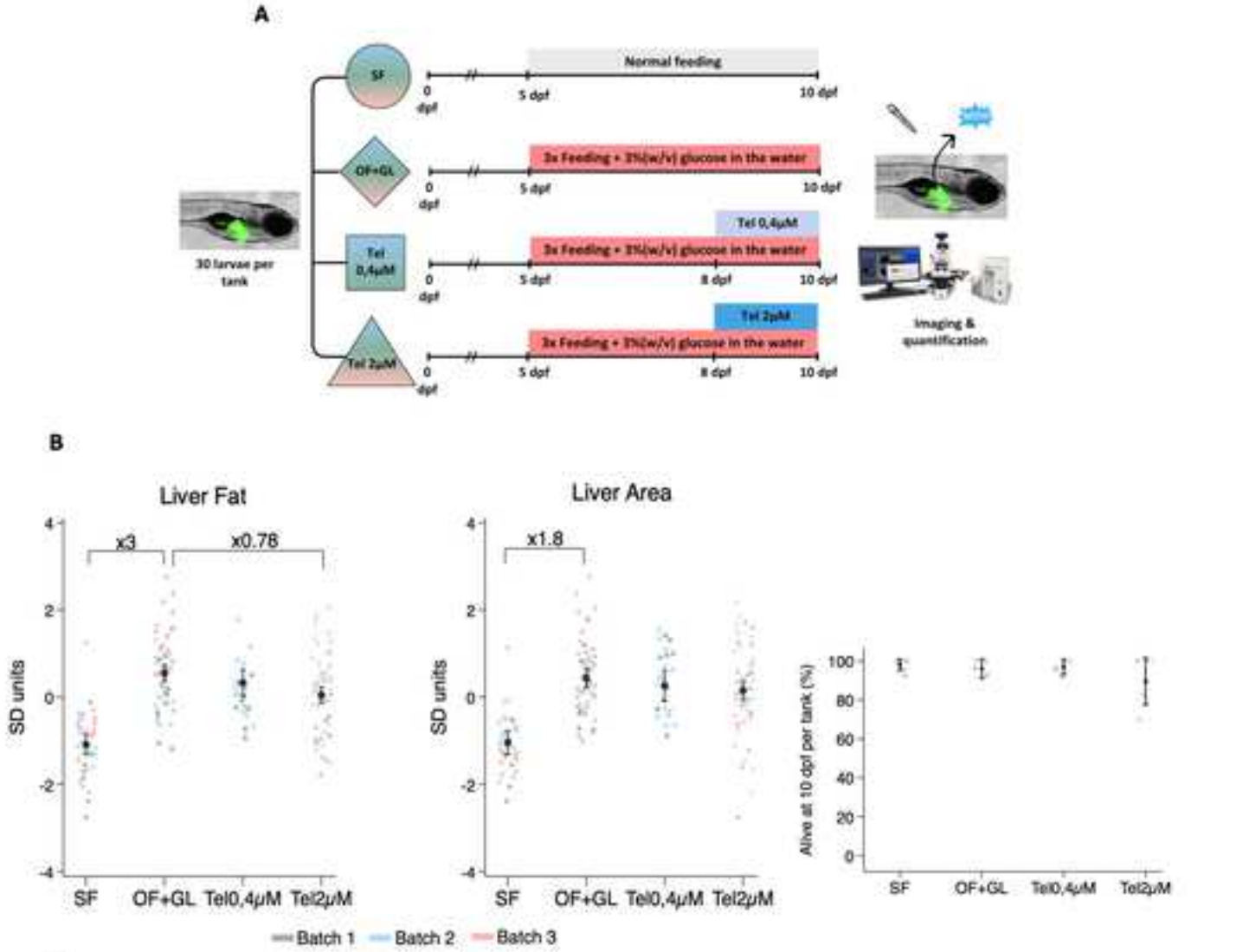

C

Groups:	SF		Tel 0,4uM		Tel 2uM	
Estimates:	Beta size and Standard Error vs OF+GL	P value vs OF+GL	Beta size and Standard Error vs OF+GL	P value vs OF+GL	Beta size and Standard Error vs OF+GL	P value vs OF+GL
Lenght	-0.298/0.170	8.03e-02	-0.340/0.193	7.92e-02	-0.413/0.155	**8.23e-03**
Dorsal Area	-0.566/0.120	**4.34e-06**	-0.516/0.136	**1.78e-04**	-0.406/0.110	**2.63e-04**
Lateral Area	-0.326/0.123	**8.64e-03**	-0.251/0.140	**7.37e-02**	-0.330/0.113	**3.94e-03**

Figure 11

Click here to access/download;Figure;Fig11.jpg

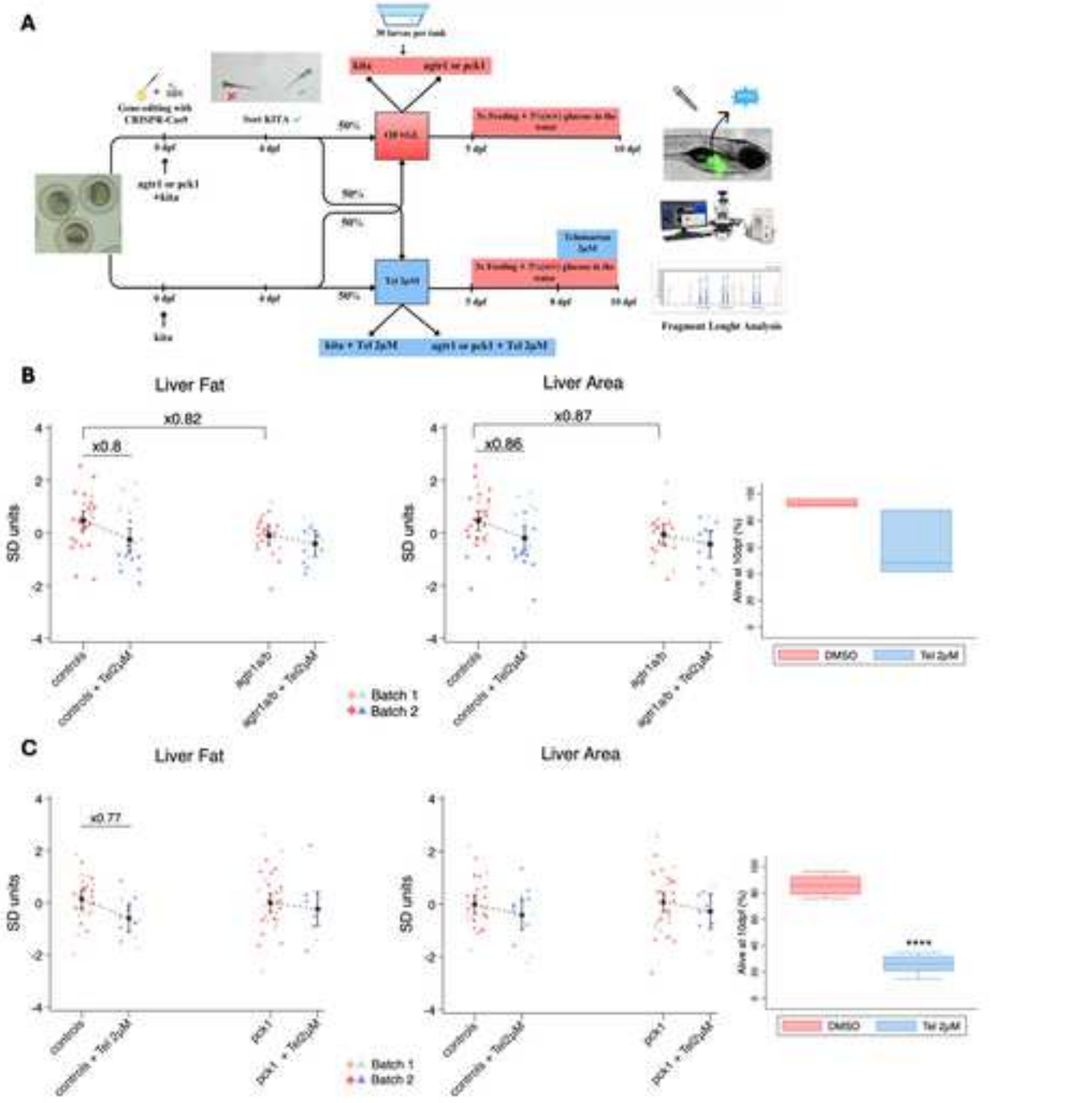

D

Groups:	Tel 2µM vs controls	
Estimates:	**Beta size and Standard Error**	**P value**
Lenght	-0.235/0.212	2.70e-01
Dorsal Area	-0.310/0.156	**4.89e-02**
Lateral Area	-0.446/0.138	**1.72e-03**

Groups:	agtr1 vs controls	
Estimates:	**Beta size and Standard Error**	**P value**
Lenght	-0.020/0.263	7.87e-01
Dorsal Area	-0.497/0.189	**1.12e-02**
Lateral Area	-0.302/0.154	**5.48e-02**

Groups:	pck1 vs controls	
Estimates:	**Beta size and Standard Error**	**P value**
Lenght	0.126/0.277	6.50e-01
Dorsal Area	0.005/0.208	9.83e-01
Lateral Area	-0.214/0.163	1.95e-01

Tel 2uM effect in mutated larvae

Groups:	agtr1 + Tel 2µM vs agtr1	
Estimates:	**Beta size and Standard Error**	**P value**
Lenght	-0.562/0.278	**5.07e-02**
Dorsal Area	-0.037/0.165	8.24e-01
Lateral Area	-0.030/0.144	8.37e-01

Groups:	pck1 + Tel 2µM vs pck1	
Estimates:	**Beta size and Standard Error**	**P value**
Lenght	-0.212/0.420	6.17e-01
Dorsal Area	-0.130/0.314	6.81e-01
Lateral Area	0.054/0.232	8.19e-01

Figure 12

Click here to access/download;Figure;Fig12.jpg

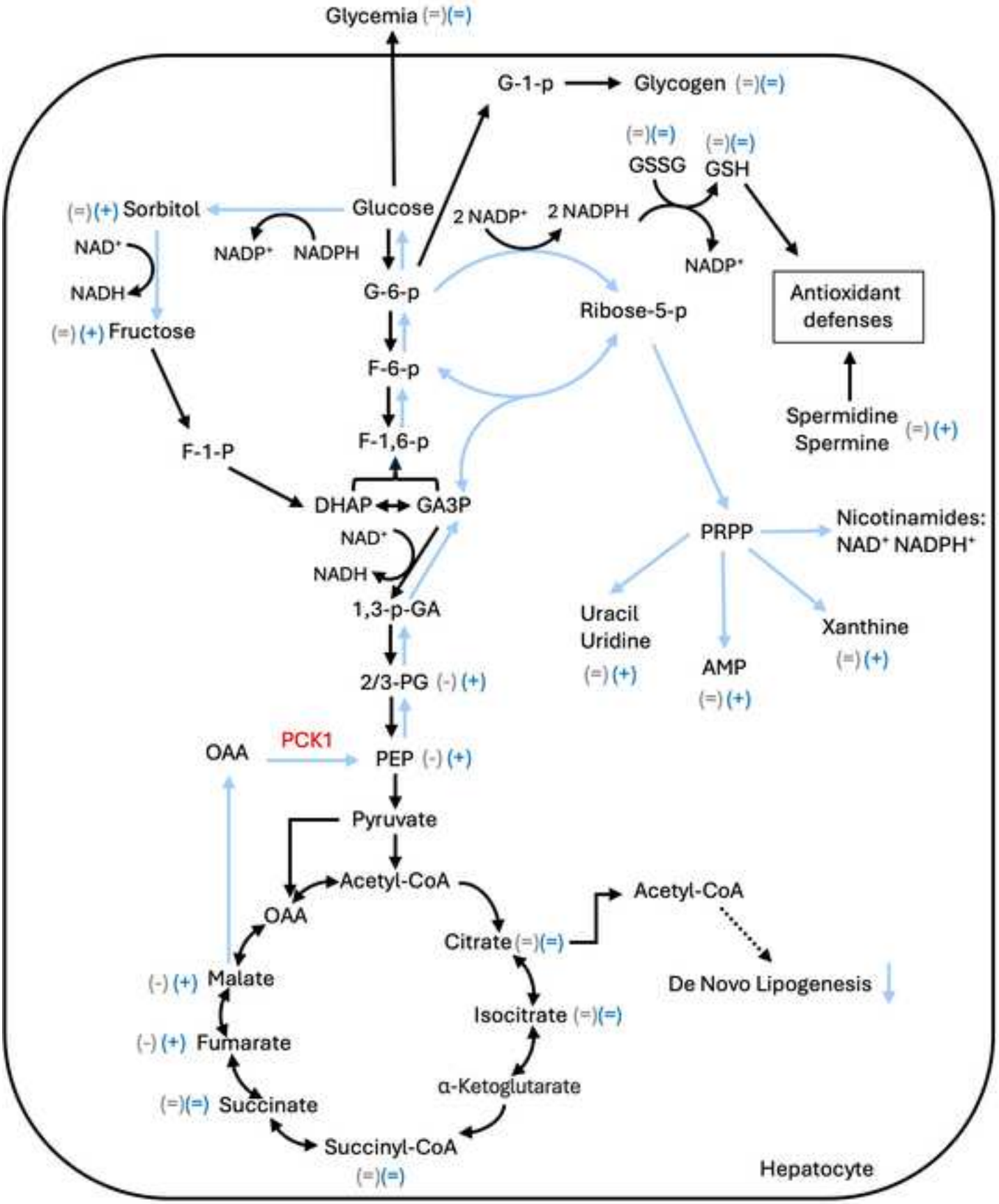

Declaration of interests

☒The authors declare that they have no known competing financial interests or personal relationships that could have appeared to influence the work reported in this paper.

☐The authors declare the following financial interests/personal relationships which may be considered as potential competing interests:

Supplementary Fig 1

Click here to access/download

Supplementary Material

Fig S1.jpg

Supplementary Fig 2

Supplementary Fig 3

Supplementary Fig 4